2

Characterization of Protein–Protein Interactions Using Atomic Force Microscopy

Hong Wang, Yong Yang, and Dorothy A. Erie*

2.1. INTRODUCTION

Atomic force microscopy (AFM), invented in 1986, expanded the application of scanning tunneling microscopy to nonconductive, soft, and live biological samples (Binnig *et al*., 1986; Hansma *et al*., 1988; Marti *et al*., 1988; Drake *et al*., 1989). AFM has several capabilities, including characterizing topographic details of surfaces from the submolecular level to the cellular level (Radmacher *et al*., 1992), and monitoring the dynamic process of single molecules in physiological relevant solutions (Drake *et al*., 1989; Engel and Muller, 2000). More excitingly, AFM not only extends our ''vision,'' but also extends our ability to ''touch and manipulate'' during our exploration of the biological system at the molecular level. For example, AFM can be used to manipulate macromolecules (Zlatanova and Leuba, 2003; Bockelmann, 2004; Gutsmann *et al*., 2004), monitor the unfolding of proteins, RNA, and protein fibers (Carrion-Vazquez *et al*., 1999; Fisher *et al*., 2000; Zhuang and Rief, 2003; Rounsevell *et al*., 2004), and measure the forces between interacting molecules (Chilkoti *et al*., 1995; Dammer *et al*., 1995; Ros *et al*., 2004). Over the past two decades, the application of AFM has advanced our knowledge in many areas of the biological sciences including DNA (Fritzsche *et al*., 1997; Hansma, 2001; Hansma

H. WANG • Laboratory of Molecular Genetics, National Institute of Environmental Health Sciences, National Institutes of Health, Research Triangle Park, NC, 27709, USA. Y. YANG • Department of Chemistry, University of North Carolina at Chapel Hill, Chapel Hill, NC, 27599, USA. D. A. ERIE • Department of Chemistry, University of North Carolina at Chapel Hill, Chapel Hill, NC 27599, USA and *Corresponding author: Tel: 919 962-6370; fax: 919 966-3675; e-mail: derie@email.unc.edu

et al., 2004), RNA (Lyubchenko *et al*., 1992; Liphardt *et al*., 2001; Abels *et al*., 2005), chromatin (Bustamante *et al*., 1997; Tamayo, 2003a,b; Zlatanova and Leuba, 2003; Leuba *et al*., 2004), proteins (Ratcliff and Erie, 2001; Stahlberg *et al*., 2001), lipids (Ikai and Afrin, 2003; Henderson *et al*., 2004), carbohydrates (Bucior and Burger, 2004), polysaccharides (Abu-Lail and Camesano, 2003), various biomolecular complexes (Lyubchenko *et al*., 1995; Bustamante and Rivetti, 1996; Bonin *et al*., 2000; Willemsen *et al*., 2000; Henn *et al*., 2001; Safinya, 2001; Janicijevic *et al*., 2003a), and cellular (Ohnesorge *et al*., 1997) and subcellular (Henderson *et al*., 2004; Jena, 2004) structures.

The main focus of this review is on the application of AFM imaging in air, which is the most widely used imaging mode. However, imaging in liquids, force spectroscopy imaging, and lateral force manipulation using AFM are briefly discussed. AFM imaging is a single molecule technique that can resolve individual protein–protein and DNA–protein complexes. For example, for studying DNA–protein interactions, an ensemble of DNA–protein complexes visualized by AFM can provide snapshots of the whole dynamic process. Furthermore, using AFM, the distribution of conformations within a complex population of molecules can be characterized (Bustamante and Rivetti, 1996). Meanwhile, multiple information, such as oligomeric state of proteins, protein-induced conformational changes in DNA, DNA-binding specificities, and DNA–protein binding constants (Yang *et al*., 2005) can be deducted simultaneously from AFM images.

This chapter focuses only on the application of AFM for investigation of protein–protein interactions free in solution and on substrates. Biological pathway events are normally implemented by protein oligomers or multiprotein assemblies rather than single proteins. If we imagine proteins as a team of workers who have jobs to do, AFM can help us understand how the players come together to bring about functions. Specifically, AFM imaging can be used to study (1) stoichiometry and protein–protein association constant (the partnership between proteins); (2) the architecture of a protein and a multiprotein complex; (3) recognition specificity of a protein complex on nucleic acids or matrix protein (the job site for a particular protein); (4) the mechanism of action of a protein, such as DNA bending or wrapping (How is the job done?); and (5) complex actions of the same or different proteins on multiple sites on DNA that result in protein filament formation, DNA looping, DNA condensation, DNA supercoiling, nucleosome remodeling, or joining of two distinct DNA molecules (How is the job done collectively?).

2.2. USE OF AFM

2.2.1. Principles of AFM

The principle of AFM varies with the different modes of AFM operation, such as contact mode, oscillating mode, and force spectroscopy mode. In the contact mode, the AFM cantilever is deflected by the sample surface. A fixed

deflection is maintained during an *X–Y* dimensional scan by adjusting the *Z* position of piezo (Figure 2.1A). The AFM image is generated by plotting the *Z* movement of the piezo as a function of the *X–Y* position. In the oscillating mode, the cantilever is oscillated by a vibration piezo. The sample surface is brought into contact with the oscillating cantilever such that it clips the amplitude of oscillation. The amplitude of this clipped oscillation, which is monitored by the laser projected on the photodiode, is maintained constant during the scan by adjusting the *Z* position of the piezo using a feedback loop. The AFM image captured in oscillating mode is generated similarly to that in contact mode; that is, by plotting the *Z* movement of the piezo as a function of the *X–Y* position. Although oscillating mode is similar to contact mode, in that the tip–surface interaction is maintained constant during an AFM scan, oscillating mode generates smaller lateral forces on the sample, which improves the lateral resolution of the AFM image on nondensely packed samples.

It is well known that due to the finite size of AFM tip, AFM imaging is a result of a tip dilation (or convolution) of the sample by the imaging tip (Figure 2.1B). Tip dilation, commonly called tip convolution, mainly refers to the contribution of size and shape of tip to the AFM image. It should be kept in mind that the spatial resolution of AFM depends on the properties of the instrument, imaging conditions, and characteristics of the samples (Bustamante and Rivetti, 1996). Consequently, there is no general definition of resolution in AFM (Bustamante and Rivetti, 1996). This argument can be supported by the fact that two objects, that can be resolved when they have nearly equal height, may not be resolved when their heights are not equal (Figure 3 in Bustamante *et al*., 1996; Yin *et al*., 1995).

2.2.2. Substrates for Sample Preparation

Flatness and biocompatibility are two basic requirements for substrates used to prepare samples for AFM imaging. Glass, mica, gold, and silicon surfaces have been used to noncovalently or covalently immobilize biomolecules (Wagner, 1998). The most commonly used substrate is muscovite mica because an atomically flat and negatively charged surface is conveniently obtained by peeling the layered mica before sample deposition. Divalent cations, such as Mg^{2+} and Ni^{2+}, can be included in deposition buffer and these divalent cations can function as salt bridges to absorb the negatively charged biomolecules such as DNA onto the mica surface (Hansma and Laney, 1996; Muller *et al*., 1997). Alternatively, chemical modification of the mica surface can be used to reverse the surface charges to extend its application (Lyubchenko *et al*., 1993; Shlyakhtenko *et al*., 2003; Podesta *et al*., 2004). In addition, lipid bilayers prepared on mica surfaces by the Langmuir–Blodgett (LB) technique can be used as substrates for the reconstitution of membrane proteins (Stahlberg *et al*., 2001). Finally, cationic lipid bilayers on mica have also been used to strongly anchor double-stranded DNA (dsDNA) to achieve high-resolution images in liquids (Mou *et al*., 1995).

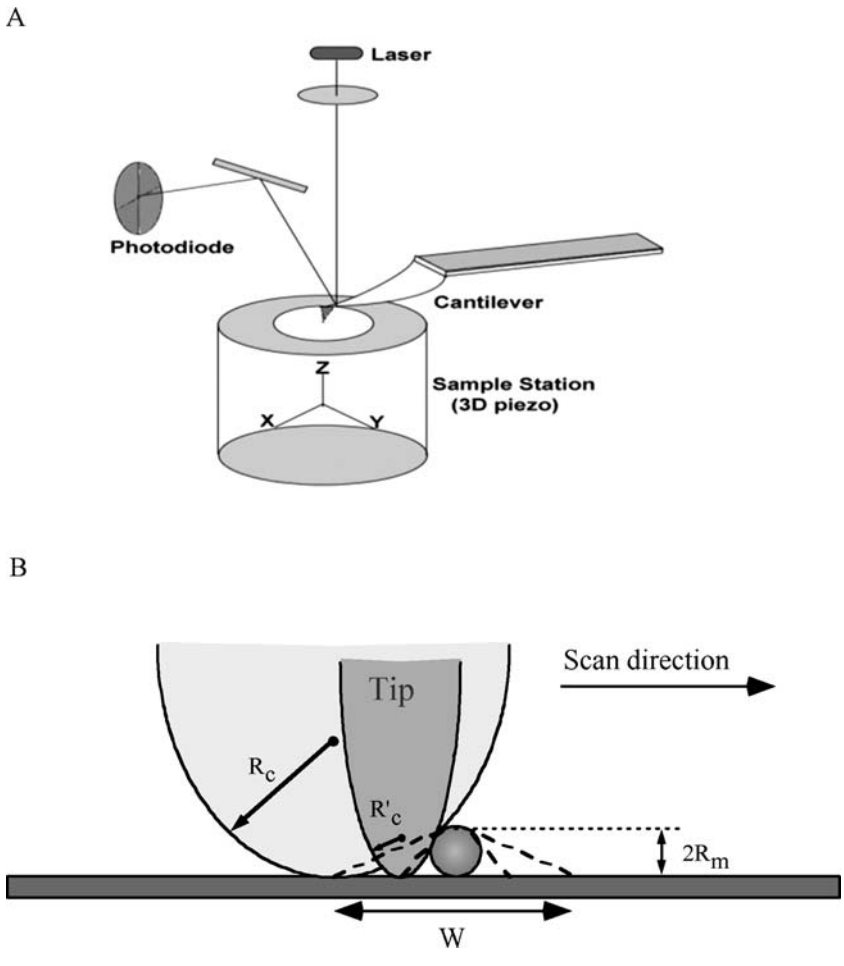

Figure 2.1. Principles of atomic force microscopy (AFM). (A) Schematic of AFM. (B) Illustration of dilation of sample by AFM tips. R_c and R'_c are the tip radii of blunt and sharp AFM tips, respectively. R_m is the half height of the particle. W is the width of the particle in the AFM image.

2.2.3. Imaging in Air

In general, imaging in air is less time consuming than imaging under solution and can provide valuable information about the structural properties of protein–protein complexes in solution and on nucleic acids or matrix proteins. For imaging in air, the sample is first deposited onto a substrate in the buffer of choice. All the water and buffer used for AFM sample storage and deposition should be filtered and screened for absence of small particles by AFM imaging before use. For preparing samples to study DNA–protein complexes, if the concentration of free protein is too

high, the DNA–protein complexes can be isolated using a spin-column method before sample deposition (Hoyt *et al*., 2001).

Samples can be incubated on the surface for up to several minutes before rinsing and drying. An immediate rinse is preferred because longer incubation on the surface increases the chance that the molecules or complexes could be altered by interaction with the surface. After deposition of the sample, the surface is rinsed with filtered distilled deionized water, excess water is wicked off using a piece of filter paper, and the surface is dried with a gentle stream of filtered nitrogen gas. Rinsing the surface is required to remove buffer components, but overrinsing could denature samples and decrease the coverage. Underdrying can reduce AFM resolution because macromolecules can move around on moist surfaces.

For sample deposition, the concentration of macromolecules in solution needs to be sufficiently diluted so that the amount of sample deposited onto the substrate surface is not too crowded. This minimizes the chance of two separate molecules coincidently landing on the same spot on the surface. For DNA, a reasonable coverage on a mica surface can be obtained with DNA concentrations in the range of $1–10\,\mu g/mL$. However, DNA coverage on mica can be dramatically affected by the buffer contents. For example, Mg^{2+} in the buffer can increase DNA coverage on the mica, but monovalent ions will decrease the DNA coverage. For proteins, the required concentration (typically $< 1\,\mu M$) varies depending on the protein. For some proteins, the protein coverage on mica is less dependent on the salt concentration compared with DNA. However, it has been shown that monovalent cations can also inhibit the adsorption of a number of different proteins onto mica (Czajkowsky and Shao, 2003). Kinetic experiments indicated that the transport of DNA molecules from the solution onto the surface is governed solely by diffusion, and analyses of protein and DNA binding to mica indicated that they bind irreversibly over the time scale of deposition (Lee and Belfort, 1989; Rivetti *et al*., 1996; Gettens *et al*., 2005). In addition, DNA molecules deposited onto freshly cleaved mica were able to equilibrate on the surface, as in an ideal two-dimensional (2D) solution (Rivetti *et al*., 1996).

It should be kept in mind that a major assumption when interpreting AFM data is that what observed on the surface is what is in solution, that is, deposition on the surface does not alter the populations or structures. In many cases, this assumption is valid. However, there are exceptions. For example, it is possible that a protein can induce a 3D topology in the DNA such that protein–DNA complex must be distorted to lie flat on the surface. If surface-induced problem is a concern, in some cases, changing to different kinds of substrate for sample deposition can minimize the problem.

2.2.4. Imaging in Liquids

Imaging samples in liquids by AFM offers several advantages over imaging in air. One obvious advantage is the ability to follow the dynamic structural changes of native single molecules, as well as the interactions between macromolecules, in

physiologically relevant buffers in real time. For imaging in liquids, a liquid chamber is needed to seal the buffer and allow for buffer exchange. A flow apparatus can be set up to facilitate the switching between different buffers and minimize the thermal drift of the instrument (Guthold *et al*., 1999b). Accessory proteins, substrates, cofactors, and inhibitors can be injected into the fluid chamber. These procedures permit one to observe dynamic conformational changes of the same single protein or the interactions between macromolecules before and after the addition of these chemical and physical factors (Oberleithner *et al*., 1996; Osmulski and Gaczynska, 2000). Accordingly, direct correlation between structural and functional states of individual biomolecules can be made. Such information can be elusive using other techniques such as electron microscopy (EM), crystallography, and AFM in air, which take static pictures of macromolecules in nonnative environments. The second major advantage of imaging in liquids is the minimal force that can be applied to the sample during imaging due to the elimination of capillary forces (Drake *et al*., 1989). Consequently, the deformation of biological samples is reduced relative to imaging in air, which is a prerequisite to high-resolution imaging of soft biological samples. For close-packed macromolecules, such as 2D crystal arrays, contact mode in liquids has generated images with lateral resolutions down to 0.41 nm and vertical resolutions down to 0.10 nm (Muller *et al*., 1998; Stahlberg *et al*., 2001; Fotiadis and Engel, 2004). To minimize possible deformation of the biological specimen by the tip, soft cantilevers with spring constants $\sim 0.1\,\mathrm{N/m}$ must be used and scanning must be done at minimal tip force (~ 100–$300\,\mathrm{pN}$) (Fotiadis and Engel, 2004). Oscillating mode in liquids is generally preferable over contact mode for imaging samples with macromolecules loosely attached to the surface. Oscillating mode minimizes lateral forces exerted by the tip and the detachment of the sample from surface during the scan. In addition, for imaging weakly bound individual macromolecules in liquids, the jumping mode, an imaging mode that has not been widely available on commercial instruments, can minimize lateral and vertical forces and has advantages over contact and oscillating modes (Moreno-Herrero *et al*., 2004). In jumping-mode AFM, at each image point, first the topography of the sample is measured during a feedback phase of a cycle, and then the tip–sample interaction is evaluated in real time as the tip is moved away and toward the sample. As the tip is controlled in such way that it moves laterally to the next point at the maximum tip–sample separation, the lateral forces that can detach the samples from surface and lower the image resolution are greatly minimized.

So far, only a small percentage of the published work done using AFM has been performed in liquids because imaging biomolecules in aqueous solutions remains challenging. First, to watch the dynamic processes in liquids, the right conditions must be identified. Specifically, the samples must bind tightly enough to the surface to allow good imaging but loosely enough to allow the interactions to occur on the surface (Guthold *et al*., 1999b; Jiao *et al*., 2001). Second, the scan rates of commercial AFMs are slow. Many biological reactions happen in the order

of milliseconds to seconds, but for commercial AFMs, it will take ~30 s to collect a 1 μm × 1 μm image at reasonable resolution (Jiao *et al*., 2001). In the past several years, however, developments have been made in both the instrumentation and the cantilevers, which have improved the reliability of the instrument and allowed faster scan rates (Han *et al*., 1996; Ratcliff *et al*., 1998; Viani *et al*., 1999; Ando *et al*., 2001; Rogers *et al*., 2004).

2.2.5. Force Spectroscopy Mode

The ability to form biomolecular assemblies is fundamentally governed by the long-range and short-range interacting forces between macromolecules. Thermodynamics and dynamics are the traditional tools for us to determine the strength of biomolecular interactions. Although the force between interacting components can be measured directly by some methods, such as the surface force apparatus, these methods lack the spatial resolution to give information at the molecular level (Florin *et al*., 1994). Recent developments on force spectroscopy mode AFM and optical tweezers opened an exciting area for understanding the strength of interactions at a single-molecule level (Bustamante *et al*., 2000). Comparing with optical tweezers, in terms of sensitivity of force measurements, conventional AFMs can detect forces in the range of 0.01–100 nN, whereas optical tweezers can exert forces in the range of 1–200 pN (Leckband, 2000). Moreover, subpiconewton forces have been resolved using specialized instrumental developments (Tokunaga *et al*., 1997). The detection limit of AFM force spectroscopy would meet the requirements needed for detecting the interacting forces in biomolecular assemblies, which are in the piconewton range (Florin *et al*., 1994; Luckham and Smith, 1998). For example, at saturating nucleoside triphosphate concentrations, RNA polymerase (RNAP) molecules stalled reversibly at a mean applied force estimated to be 14 pN (Yin *et al*., 1995).

For force measurement, one interacting partner is attached to the AFM tip using techniques such as chemical coating and biological functionalizations (Figure 2.2; Colton *et al*., 1998). The interaction between AFM tips and surfaces is recorded as force curves when the tip approaches or retracts from surfaces (Zlatanova *et al*., 2000). The absolute force can be deduced from the spring constant of cantilevers using established force laws [see Heinz and Hoh (1999) for review]. AFM force spectroscopy has been applied in many biological areas, such as protein–DNA, antigen–antibody pairs, protein–ligand, protein–membrane, and protein–cell interactions. A detailed review on these applications is out of the range of this chapter and some excellent reviews are available elsewhere (Clausen-Schaumann *et al*., 2000; Leckband, 2000).

Although force spectroscopy has powerful capabilities, some limitations exist in current force spectroscopy applied in biological investigations. The force measurements are so sensitive to the sample preparation and the conditions of measurements that it is difficult to compare the absolute forces obtained by different groups. Consequently, monitoring how the force changes with conditions, such as the

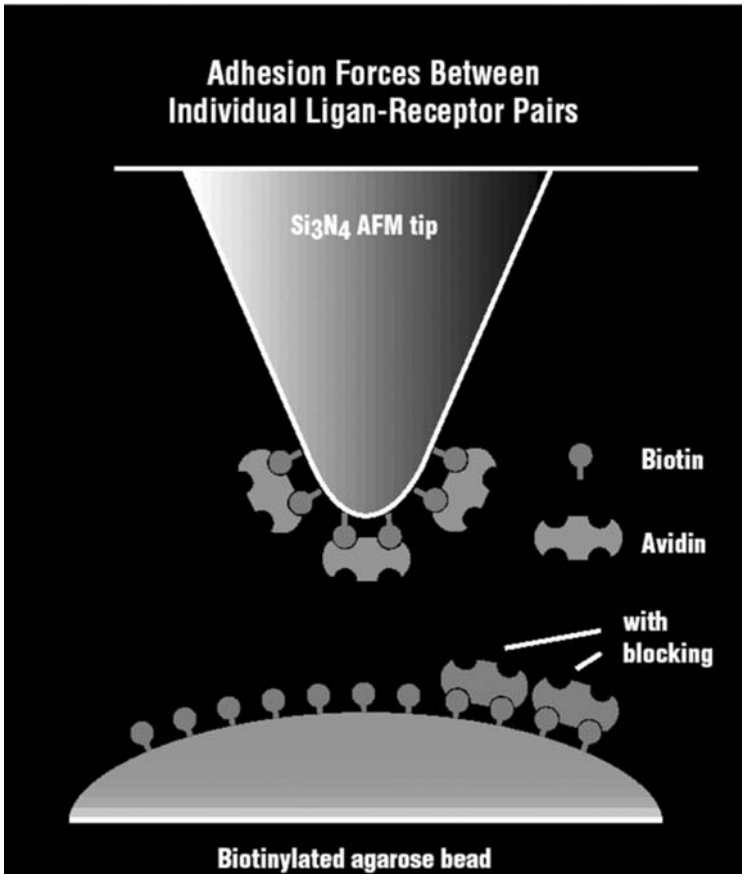

Figure 2.2. A schematic view of force spectroscopy mode. One partner (Avidin) in biomolecular interactions is attached to the atomic force microscopy (AFM) tip. Another partner (Biotin) is immobilized on the surface. The figure is reproduced from Florin *et al*. (1994) with permission.

conditions of the measurement and the buffer, is a more reliable way to understand molecular interactions in cell biology than measuring absolute force values.

2.2.6. Lateral Force Manipulation

Besides stretching the molecules using force spectroscopy mode to learn about the mechanical properties of macromolecular assemblies, AFM can also be used to manipulate sample using the lateral force with a specialized system, called nanoManipulator. The nanoManipulator system integrates the AFM with a virtual–reality interface that gives investigators new ways of interacting with objects at the nanometer scale (Guthold *et al*., 1999a, 2000; Sincell, 2000).

Using a force-feedback pen, the user can touch the surface and directly manipulate the object. The manipulation is accomplished by exporting the data to a PHANTOM controller (SensAble Technologies, Cambridge, MA). This procedure allows the investigators to precisely locate the objects and features by feel whereas the tip makes the modification. Samples can be manipulated in contact mode and the changes before and after manipulation can be monitored using oscillating mode imaging. Samples can be bent, translated, rotated, and dissected. Mechanical properties of biological samples can be measured directly by recording the vertical and lateral forces during the manipulation process. The rupture forces of fibrin (see discussion in Section 2.3.6 and Figure 2.9) and DNA have been measured using nanoManipulator, and nonspecific binding between adenovirus and silicon surface has been monitored (Guthold *et al*., 2000, 2004). Forces ranging from a few piconewtons to several micronewtons can be measured using the nanoManipulator, expanding the range of forces ($10^{-9}-10^{-14}$ N) measured by other single-molecule manipulation techniques, such as microneedles, flow field, magnetic field, and optical tweezers (Bustamante *et al*., 2000). Compared with other single-molecule manipulation techniques, the nanoManipulator has the advantages of easy sample preparation and the ability to monitor the sample before and after the manipulation. One disadvantage of this technique is that the surface interaction may complicate the interpretation of the data. Besides measuring the physical properties of biological samples, in the future, the nanoManipulator maybe used as a tool to push the macromolecules together and watch the interaction in real time in liquids.

2.2.7. Postprocessing of AFM Images and Generating Quantitative Data

Importantly, the conclusion on the properties of protein or protein–protein complexes should be based on the analysis of statistically significant number of images collected from different depositions. Processing and quantitative analysis of AFM images are straightforward. The software-controlling AFM instruments, such as the Nanoscopes of Digital Instruments, Inc. (Santa Barbara, CA), can accomplish diverse tasks. For example, the images can be flattened to smooth the image. In addition, there are analysis tools to measure the contour length and bend angles of molecules such as DNA, as well as the height and volume of molecules. Additional software, such as Image SXM (http://reg.ssci.liv.ac.uk/) and NIH Image, are useful for the quantitative analysis of the size and the shape of molecules and complexes (Ratcliff and Erie, 2001). Image SXM allows raw image files to be opened without losing image information.

One-by-one measurements of DNA contour lengths and bend angles made by tracing each molecule using Nanoscope software is tedious and time consuming. To address this problem, custom software has been developed to automate the process. For example, a custom program written in MATLAB (Mathworks, Natick, MA) has been developed to increase the efficiency of measuring the DNA contour lengths and DNA bend angles induced by protein binding (Wang *et al*., 2003).

2.3. CHARACTERIZATION OF PROTEIN–PROTEIN COMPLEXES

2.3.1. Characterization of Protein–Protein Interactions Based on Size Information

The heights of proteins as measured by AFM can be affected by various factors, such as the orientation of proteins on the surface and electrostatic interactions between macromolecules and the tip (Muller and Engel, 1997). However, the volumes of proteins in AFM can be used to compare protein size and derive useful information, such as evidence for protein–protein association and protein–protein equilibrium association constants (K_a) (Wyman *et al*., 1997; Schneider *et al*., 1998; Ratcliff and Erie, 2001; Yang *et al*., 2003; Schlacher *et al*., 2005).

The detailed procedures for volume analysis using Image SXM were described in the supplementary information section of Ratcliff and Erie (2001). Briefly, the first step in image analysis is to determine the height of the surface (S), which is generally nonzero. This surface height must be subtracted from the measured height of each protein before volume determination (Ratcliff and Erie, 2001). After the surface height is measured, each protein is then highlighted individually using the density slice utility in Image SXM. The density slice selects the pixels above the surface that represent the proteins to be analyzed. The image analysis function in Image SXM scans the image and selects all the highlighted proteins within the density slice. Analysis of each protein within the slice is then performed. In addition to height and area information, which permit the calculation of the protein volume, Image SXM can calculate the major and the minor axes by fitting the cross section of each protein to an ellipse. The volume for each protein, V_i, is calculated by multiplying the area, A_i, by the corrected average height (total average height, M_i, minus surface height, S)

$$V_i = A_i(M_i - S).$$

It has been shown using a large number of proteins that there is a quantitative linear dependence of the protein volume measured from AFM images on the molecular mass of proteins (Wyman *et al*., 1997; Schneider *et al*., 1998; Ratcliff and Erie, 2001; Figure 2.3). Consequently, volume analysis is a robust and reliable method to obtain the stoichiometries of protein–protein assemblies (Schneider *et al*., 1998; Ratcliff and Erie, 2001). In addition, it is possible to use this volume analysis to determine homo- or heteroprotein–protein equilibrium association constants (K_a). This methodology has been used to determine the equilibrium association constant for the dimerization of *Escherichia coli* DNA helicase II (UvrD), in which the shifts in the distribution of protein oligomeric states under different protein concentrations were analyzed (Figure 2.4A and B; Ratcliff and Erie, 2001). Recently, analysis of protein volumes from AFM images directly revealed the DNA-independent interaction between pol V and RecA (Figure 2.4C; Schlacher *et al*., 2005). The conclusion is based on the observation that incubation of RecA and pol V together resulted

in the formation of particles with a larger average volume than that seen with either protein alone (Figure 2.4C; Yang *et al*., 2003; Schlacher *et al*., 2005). It is worth noting that the observed AFM volume of pol V–RecA complex is consistent with the predicted volume of pol V–RecA protein complex based on the standard curve shown in Figure 2.3. The direct interaction between pol V and RecA observed in AFM is a key observation supporting the idea that the role of RecA is not simply to target pol V to a stalled replication fork. Instead, RecA directly activates pol V, possibly as a subunit of the active pol V holoenzyme complex in translesion DNA synthesis (Schlacher *et al*., 2005).

AFM volume analysis is also useful for determining the oligomeric state of proteins on DNA (Wyman *et al*., 1997; Xue *et al*., 2002; Bao *et al*., 2003). For example, the effects of phosphorylation and mutation of nitrogen regulatory protein C (NtrC) from *Salmonella typhimurium* on the oligomeric state of NtrC at its specific DNA recognition site have been studied using volume analysis (Wyman *et al*., 1997). This study provided evidence that large oligomers of NtrC are important for activating transcription (Wyman *et al*., 1997). In another example, the oligomeric state of hWRN-N, a fragment of human WRN gene product, has been studied using AFM volume analysis (Xue *et al*., 2002). The study showed that hWRN-N is in a trimer–hexamer equilibrium in the absence

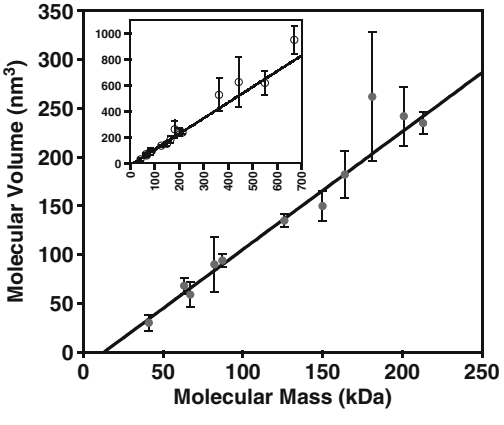

Figure 2.3. Plot of protein volume versus molecular mass. The volumes were determined as described in reference (Ratcliff and Erie, 2001). Data are shown for 15 proteins and protein–protein complexes. In the main plot, there are alcohol dehydrogenase (41 kDa), hWRN-N_{70-240} trimer (63 kDa), bovine serum albumin (67 kDa), UvrD monomer (82 kDa), PCNA trimer (87 kDa), hWRN-N_{70-240} hexamer (126 kDa), hWRN-N_{70-240} trimer, PCNA trimer complex (150 kDa), UvrD dimer (164 kDa), *Taq* MutS dimmer (181 kDa), β-amylose (201 kDa), hWRN-N_{70-240} hexamer, and PCNA trimer complex (213 kDa). The insert plot also includes *Taq* MutS tetramer (362 kDa), apoferritin (443 kDa), RNA polymerase (RNAP) (550 kDa), and thyroglobulin (670 kDa). The line represents the weighted least-square fit of the data, which is described by the equation $V = 1.2(\mathrm{MW}) - 15.5$, where V is atomic force microscopy (AFM) volume and MW is molecular weight ($R^2 = 0.983$). The error bars represent the standard deviation of the distribution for each protein. The data are taken from references (Ratcliff *et al*., 1998 and Yang *et al*., 2003) and unpublished results.

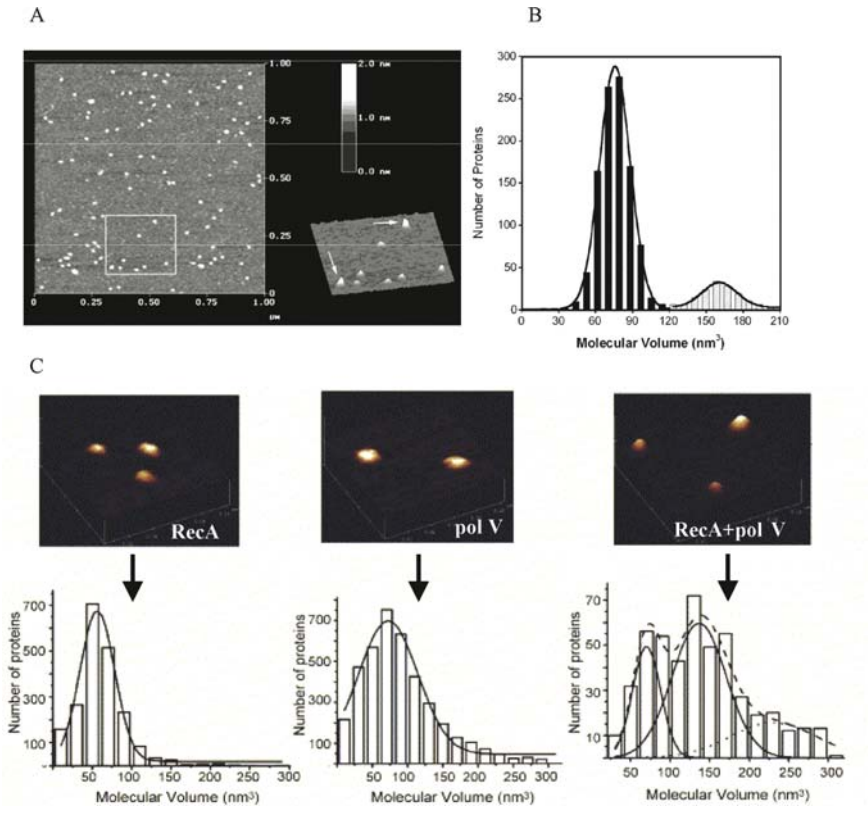

Figure 2.4. Using atomic force microscopy (AFM) volume analysis to investigate oligomeric states of proteins and protein–protein interactions. (A) AFM image of UvrD at 50 nM. The image shows proper surface coverage for volume analysis. The surface plot (inset) represents the rectangle area within the image. Arrows in the inset point to dimers; the other proteins within the inset are monomers. Image is reproduced from Ratcliff and Erie (2001) with permission. (B) Gaussian fits of the volume histogram for UvrD (250 nM). The solid lines are Gaussian fits of the volume data for monomers (solid bars) and dimers (hatched bars). Each species was fit independently. The number of proteins under each curve represents the species' population. Plot is reproduced from Ratcliff and Erie (2001) with permission. (C) AFM images of RecA, pol V, and pol V–RecA complexes. The image size is 100 nm × 100 nm for all images. The arrows point to the volume distributions for each protein. A Gaussian distribution was calculated for each data set and is displayed as a solid black line. For the pol V–RecA complexes, the distinct peaks from the Gaussian function are displayed as solid black lines and the distribution for all peaks is displayed as dashed lines. Images and plots are reproduced from Schlacher *et al*. (2005) with permission.

of DNA, but it is primarily hexamer, the active form for its functions, in the presence of DNA substrates.

AFM volume analysis is useful to study the protein–protein association because it can be complementary to other techniques. For example, analytical ultracentrifugation and isothermal titration calorimetry require high concentrations of samples, which would limit their use in assaying proteins with low solubility or

with tight-binding constants. In addition, sample deposition for AFM imaging can be done over a wide range of temperature ranges on a hot plate, which is advantageous for studying thermophilic proteins.

Although volume analysis is a powerful method for determining protein stoichiometries and protein equilibrium association constants, care must be taken when acquiring the images (Ratcliff and Erie, 2001). First, the tip geometry and the strength of the tip–surface interactions need to be consistent in all the experiments, because AFM images are the convolution of tip–surface interactions. Standard curves relating AFM volume and molecular weight of protein may need to be generated in each laboratory using different AFM instruments. It is highly recommended to use a new cantilever each time when collecting final images for volume analysis purpose. Alternatively, another protein with known size close to the protein of interest can be added to the protein sample as a size standard (Verhoeven *et al*., 2002). In addition, when imaging the DNA–protein complex, the AFM volume of DNA can be used to normalize the AFM volume of proteins (Wang, 2003). It should also be kept in mind that factors that affect the surface deposition of proteins may influence the measured association constant (Ratcliff and Erie, 2001). Two major factors are interaction of the proteins with the surface and diffusional properties of the proteins. If the oligomerized protein diffuses significantly more slowly than the monomer, its population could be underrepresented in an AFM image when very short deposition times are used. This effect would decrease the apparent association constant. Fortunately, diffusional factors should only become important for higher-order oligomers, because the diffusion coefficients of globular proteins depend inversely on the cube root of their molecular weights. Finally, it is worth mentioning that the use of volume analysis is not easily applicable to proteins whose molecular mass is <20 kD because of the limitation of AFM resolution.

2.3.2. Characterization of Architectures of Proteins and Protein–Protein Complexes

Even though AFM imaging cannot provide structural information on protein at atomic level, it can provide a unique view into the architecture of protein and protein–protein complexes. Thus, structural information from AFM images can further our understanding of structure–function relationship of proteins.

The human Rad50–Mre11 complex has important functions in double-strand break repair. AFM imaging revealed a central globular domain from which two long thin structures (arms) extended (Figure 2.5A–F; de Jager *et al*., 2001). Based on AFM images, along with sedimentation equilibrium data suggesting that the Rad50–Mre11 complex consists of two Rad50 and two Mre11 molecules, an intermolecular coiled-coil structure has been proposed (de Jager *et al*., 2001). In addition, AFM images of Rad50–Mre11 complexes on DNA showed an important role of the arms of Rad50–Mre11 in bridging two DNA fragments (see more discussion in Section 2.3.5; de Jager *et al*., 2001).

AFM imaging has also been used to investigate the multisubunit $GABA_A$ receptor, which is the major inhibitory neurotransmitter receptor in the brain (Edwardson and Henderson, 2004). It is known that all these receptors have a common structure, with five subunits arranged around a pseudo fivefold axis. However, there are six possible subunit arrangements in a $GABA_A$ receptor of stoichiometry $2\alpha:2\beta:\gamma$ (Figure 2.5G). The physiological relevant arrangement of the subunits around the receptor rosette has not been established. In one study, a hexahistidine (His_6) tag was attached onto the C-terminus of the α-subunit and the purified receptors containing all three subunits were incubated with an anti-His_6 immunoglobulin G (Edwardson and Henderson, 2004). The resulting receptor–immunoglobulin G complexes were imaged by AFM (Figure 2.5H). AFM images revealed that the most common angle between the two antibody tags was 135° (Figure 2.5I), close to the expected value of 144° if the two α-subunits are separated by a third subunit. This result excludes three (arrangements 3, 4, and 6 in Figure 2.5G) of the six possible arrangements of the subunits around the receptor rosette for majority of the $GABA_A$ receptors. Meanwhile, a small percentage of the complexes has an angle of 75° between the two bound antibodies (Figure 2.5I), suggesting the receptor has a mixed population of configurations. The understanding of the architecture of the $GABA_A$ receptor will help to design drugs with higher specificity (Edwardson and Henderson, 2004).

As mentioned earlier, AFM imaging in air using commercial microfabricated AFM cantilevers has generated useful information on the architecture of some proteins (de Jager *et al*., 2001; Edwardson and Henderson, 2004). However, expansion of the application of AFM to study the architecture of more proteins depends on higher-resolution images. It is well established now that besides instrumental factors, major factors that can affect the quality of the image include the shape of the tip, tip–sample interactions, stable immobilization of the sample on the surface, as well as the pH and the ionic strength of the buffer used for absorbing and scanning the sample (Mou *et al*., 1995; Muller and Engel, 1997; Muller *et al*., 1999; Hafner *et al*., 2001). At room temperature, easy deformation by the scanning tips and the thermal motion of most macromolecules make it hard to achieve high-resolution images. Close packing of the sample on the surface can reduce this problem to some degree, and subnanometer resolution images have been acquired on these samples by imaging in liquids (Muller *et al*., 1998, 2001; Stahlberg *et al*., 2001; Conroy *et al*., 2004). Cryo-AFM holds the promise for imaging a large variety of biological samples at high resolution, comparable with EM (Shao and Zhang, 1996; Shao *et al*., 2000; Sheng and Shao, 2002; Sheng *et al*., 2003). Meanwhile, even with the state-of-art techniques such as cryo-AFM, the resolving power of AFM will not be fully reached without a well-defined ultrasharp tip. Carbon nanotube tips are the most promising candidates for the next generation of ultrasharp AFM probes (Woolley *et al*., 2000; Hafner *et al*., 2001). Next, we discuss some examples of high-resolution AFM images achieved on 2D protein crystals and using carbon nanotube tips.

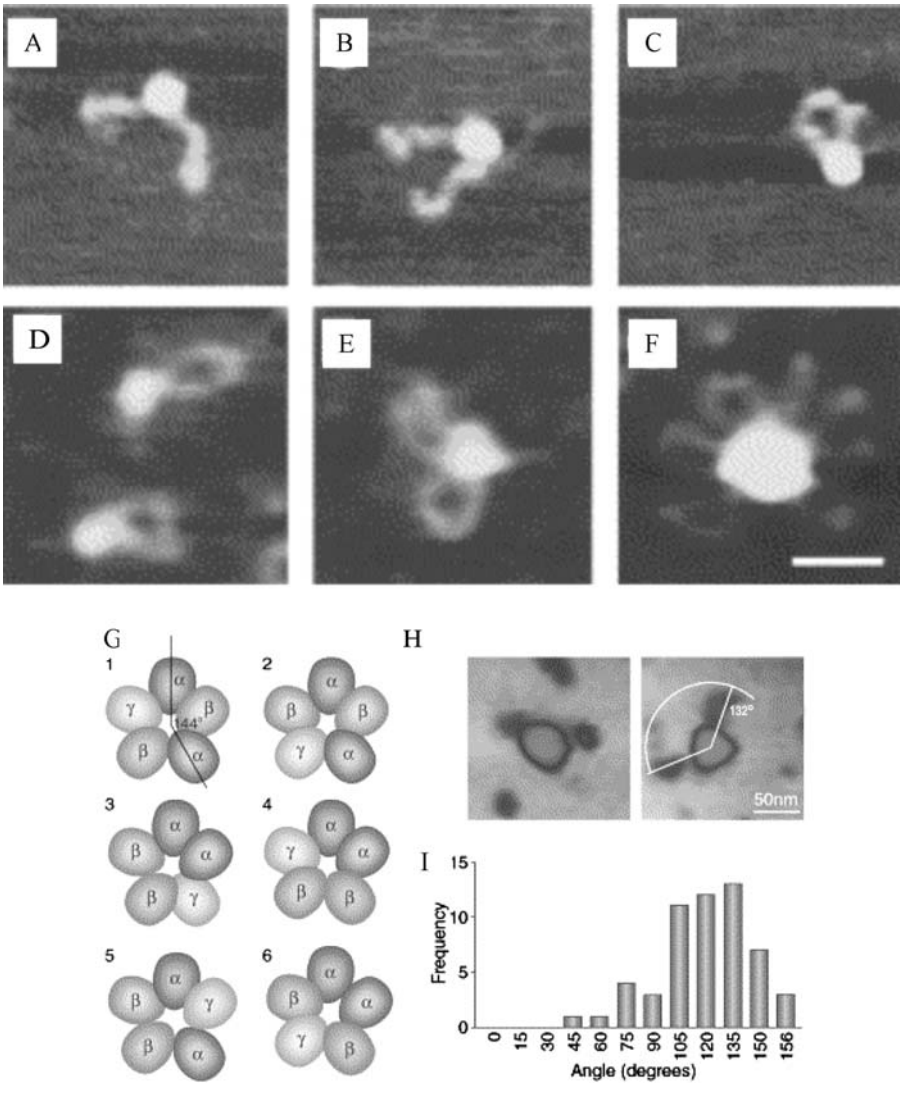

Figure 2.5. Using atomic force microscopy (AFM) imaging to study the architectures of protein complexes. (A–F) Representative AFM images of human Rad50–Mre11 complexes captured by tapping mode in air. Rad50–Mre11 exhibited a distinct architecture with a central globular domain from which arms of 40–50 nm protruded. The arms were observed in a variety of conformations. Images are reproduced from de Jager *et al*. (2001) with permission. (G–I) Analysis of $GABA_A$ receptor architecture by AFM. (G) Possible arrangements of subunits in a $GABA_A$ receptor composed of 2α-, 2β-, and 1γ-subunits. (H) AFM images of complexes between $GABA_A$ receptors, with His_6 tags on their α subunits, and mouse monoclonal anti-His_6 immunoglobulin G molecules. (I) Distribution of angles between antibody molecules in complexes between $GABA_A$ receptors and anti-His_6 immunoglobulin G. Note that the histogram has a major peak at 135° and a possible minor peak at 75°. (G–I) are reproduced from Edwardson and Henderson (2004) with permission.

Due to limited hydrophilic surfaces, membrane proteins do not readily form 3D crystals for X-ray crystallography. However, 2D membrane protein crystals reconstituted in the presence of lipids are more stable, and a large number of membrane proteins have been crystallized in this manner. Electron crystallography of 2D crystals has provided static structural information at atomic resolution (Stahlberg *et al*., 2001). Imaging in liquids using AFM provides an advantage over EM, in that the native environments and biological activities of these membrane proteins can be preserved throughout sample preparation and scanning. AFM is the only technique that gives insights into the surface structures and the dynamics of membrane proteins at subnanometer resolution. The high resolution is partly due to the elimination of capillary forces (Drake *et al*., 1989). Müller *et al*. demonstrated that by adjusting the pH and the electrolytes in the buffer, electrostatic double-layer repulsion between the tip and the sample can be reduced, resulting in reduced vertical and lateral forces between the AFM tip and the sample (Muller *et al*., 1999). In addition, the 2D crystals are strongly anchored to the substrates in liquids, and the force applied to the AFM tips is believed to be distributed over a large sample area on these 2D crystals. The factors mentioned collectively earlier dramatically reduce the sample deformation during scanning. In addition, only the small sharp protrusion at the end of tip is believed to sense the short-range electrostatic repulsion that confers high-resolution structural information. Subnanometer resolution imaging has been demonstrated by the images of purple membrane (which consists of bacteriorhodopsin and lipids) (Muller *et al*., 1999). A lateral resolution of 0.6 nm (width at half-maximum height) is reproducible in these images.

Carbon nanotubes further extend the power of AFM as a tool to characterize architecture of proteins. Carbon nanotubes have advantage over the microfabricated probes due to their small radii (0.7–5 nm for single-walled nanotubes), high aspect ratio, extremely large Young's modulus (stiffness), and the ability to be elastically buckled under large load. There are several elegant reviews on the fabrication technologies and high-resolution imaging using carbon nanotubes (Stevens *et al*., 2000; Woolley *et al*., 2000; Hafner *et al*., 2001). For example, using carbon nanotubes, the two sides of GroES, a component of the GroEL–GroES chaperonin system involved in protein folding, have been resolved (Hafner *et al*., 2001). One side was seen as a ring-like structure with an 11-nm outer diameter and the other face looked like a dome with the same diameter. In future, it is possible that carbon nanotube AFM tips will make it routine to obtain images at nanometer resolution.

2.3.3. Characterization of Recognition Specificities of Proteins

The first step for many proteins to participate in DNA transaction events is the recognition of specific sites, such as a DNA replication origin sequence, promoter region, a DNA damage or mismatch. Traditionally, bulk solution measurements, such as electrophoretic mobility-shift assays (EMSA), filter-binding assays, surface plasmon resonance (SPR), and calorimetric assays are used to

study the DNA–protein binding affinity and specificity. The limitation with these bulk solution methods is that the observed affinities are the weighted sum of all interactions, including the specific, the nonspecific, and the DNA ends (if a linear fragment is used). These bulk assays can only determine the apparent binding constants to the entire DNA fragment. For example, if a protein has significant binding affinity for the DNA ends, the apparent binding constant to short linear DNA fragment measured by bulk assays would obscure the true specificity to specific sites. Visualization of protein on DNA by AFM not only provides information on the extent of binding of protein to a DNA fragment, but also on where the protein is bound to DNA. In addition, for AFM imaging in air, the DNA–protein complex present in the reaction mixture at the time of deposition is fixed on the surface for imaging. Therefore, it is possible to observe DNA–protein complexes that might dissociate in gel electrophoresis-based assays (de Jager *et al*., 2001).

From the earlier work using AFM, it is appreciated that indeed AFM can be used to identify the specific recognition site of a protein on DNA or on an extracellular matrix protein (Erie *et al*., 1994; Allison *et al*., 1996). This identification is achieved by looking at the position distribution of the protein on the DNA or a matrix protein, which have one or more specific recognition sites at defined locations (Figure 2.6). For example, AFM was used to investigate the binding of Factor IX, a 57-kDa zymogen of a serine protease that participates in blood coagulation, to Collagen IV (Wolberg *et al*., 1997). Collagen IV is an extracellular matrix protein and a major component of the basement membrane region of endothelial cells. In this study, antibody A-5 was used to increase the apparent size of Factor IX to make it more easily identifiable on Collagen IV. Figure 2.6A shows a representative AFM image of Factor IX–A-5 complex bound to Collagen IV. In addition, Wolberg *et al*. identified two specific binding sites by plotting the position distribution of Factor IX–A-5 complexes on Collagen IV (Figure 2.6B).

In principle, for a linear substrate, the distribution of positions of the protein on the substrate provides a direct measurement of binding affinity to specific and nonspecific sites. Recently, the theoretical basis for rigorous analysis of DNA–protein complexes from AFM images to estimate specific and nonspecific DNA-binding constants and specificities has been worked out (Yang *et al*., 2005). Using this analysis on the previously published data on human DNA damage recognition protein XPC-HR23B and human 8-oxoguanine DNA glycosylase (hOGG1) demonstrated that for proteins with high specificity, methods based on AFM images yield similar numbers of binding specificity compared with bulk biochemical assays (Chen *et al*., 2002; Janicijevic *et al*., 2003b; Yang *et al*., 2005). However, this new study demonstrated that in the case of protein that has high affinity to DNA ends, compared with bulk solution measurement, single molecule methods based on AFM images can provide more accurate measurement of a binding constant to an individual site (Yang *et al*., 2005). Based on EMSA, the specificity of *Taq* MutS, which is involved in DNA mismatch recognition, for a T-bulge on a short DNA fragment is $\sim$1700; whereas, it is only $\sim$30 for *E. coli* MutS. AFM imaging and statistical analysis revealed that *E. coli* MutS binds to

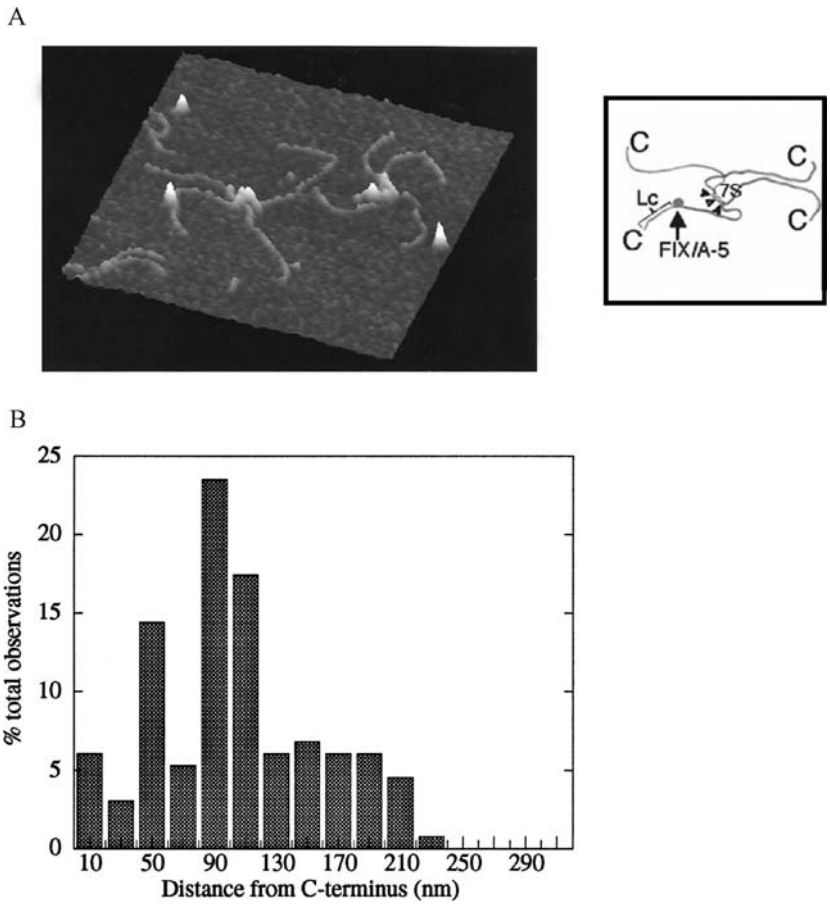

Figure 2.6. Using atomic force microscopy (AFM) imaging to study the binding specificity of proteins. (A) Surface view of Factor IX–A-5 complexes bound to Collagen IV C termini. 7S domains and Factor IX–A-5 complexes are indicated in the diagram on the right-hand side of the image. (B) Distribution of distances of the Factor IX–A-5 complexes from the free (C-terminal) end of the Collagen IV monomers. Both the peaks (located at 98 ± 13 nm and 50 ± 13 nm, respectively) were statistically significant ($p < 0.0004$). The larger peak at 98 nm likely represents a high-affinity, specific Factor IX binding site on the collagenous domain, whereas the smaller peak may represent a secondary, specific Factor IX binding site, which has threefold to fourfold lower affinity for Collagen IV than the primary site. Image and plot are reproduced from Wolberg *et al*. (1997) with permission.

DNA ends with an affinity that is only approximately five times less than that to a GT mismatch. This study suggested that the apparent differences in specificity of *Taq* and *E. coli* MutS for a T-bulge determined from bulk measurements likely result from differences in the extent to which end binding is being detected in bulk assays. In summary, the binding specificities observed from AFM are more

accurate. Specifically, AFM provides a direct measure of the relative affinities for the different sites on individual DNA fragments; whereas, bulk assays yield relative affinities of a protein to different DNA fragments. Protein-binding specificity to DNA ends is also of great interest, because DNA ends are common intermediates in genome metabolism and can be caused by endogenous and exogenous DNA-damaging agents. Failure to correctly process these DNA ends can lead to mutations, uncontrolled cell growth, and carcinogenesis. It has been discovered that to prevent these detrimental effects of DNA ends, some proteins can recognize DNA ends and function as DNA damage sensor and recruit other protein factors for further processing of DNA ends. AFM imaging provides direct evidence that some proteins indeed preferentially bind to DNA ends. The examples are Rad50 and Mre11 (R–M) complex, ataxia-telangiectasia gene product ATM, MutS, and DNA-dependent protein kinase (DNA-PK) (Yaneva *et al*., 1997; Smith *et al*., 1999; de Jager *et al*., 2001, 2002).

It is worth mentioning that although both selective and systemic alterations in the DNA occupancy by the surface can affect the absolute constants measured by AFM method, only biased alterations between the occupancy on the specific site and that on nonspecific sites will affect specificities. There are more detailed discussions on this subject in Yang *et al*. (2005).

AFM imaging also makes it possible to observe multiple recognition events on distinct sites on the same DNA fragment or on an extracellular matrix protein (Allison *et al*., 1996; Gaczynska *et al*., 2004). For example, in eukaryotes, the initiation of DNA replication depends on the recognition of origin sequence by the origin recognition complex (ORC), a heteromeric six-subunit protein complex. Gaczynska *et al*. used AFM to examine the binding of *Schizosaccharomyces pombe* (*sp*) ORC to the *sp* autonomously replicating sequence 1 (*ars1*) and found two binding sites in *ars1* (Gaczynska *et al*., 2004). Although one binding site discovered in this study was consistent with previous studies, another binding site was not previously identified. In addition, by using each single subunit of *sp*ORC and mutant proteins, AFM imaging further identified one of the six subunits of *sp*ORC and its structural element that is responsible for binding to *ars1*. This study is a good example showing that AFM can be used as a great tool for studying recognition events involving multiple sites, such as transcription and replication initiation processes.

For mapping the binding sites of protein on circular DNA, the challenge is to add a position marker on circular DNA. Site-specific labeling of covalently closed circular DNA has been achieved by using triple helix-forming oligonucleotides (Zelphati *et al*., 2000). The binding of avidin or streptavidin to a biotin group on the oligonucleotide probes can serve as a position marker. In addition, two approaches have been described for stably conjugating peptides, proteins, and oligonucleotides onto plasmid DNA (Zelphati *et al*., 2000). Recently, the Lyubchenko group used an inverted repeat sequence, which forms a cruciform as a position marker to study the binding of the Zα domain of human ADAR1 on a supercoiled plasmid (Lushnikov *et al*., 2004).

2.3.4. Characterization of Mechanisms of Action of Proteins on DNA

AFM can not only be used to investigate the partnership between proteins, but also to provide information on their mechanisms of action, because each DNA–protein complex in AFM image is a snapshot of protein caught in action on DNA. In addition, using AFM to investigate protein-induced conformational changes in DNA is straightforward because the topographic difference between proteins and DNA is obvious in an AFM image.

Large conformational changes in both proteins and DNA can occur when proteins bind to DNA or exchange between specific sites and nonspecific sites. Sequence-dependent DNA helix deformability is an important component of recognition of specific sequence on DNA, alongside the more generally recognized patterns of hydrogen bonding (Dickerson, 1998). For sequence-specific enzymes, such DNA deformation, may contribute to the correct assembly of active site residues and provide access to specific DNA moieties. In addition, protein-induced DNA bending and wrapping play an important architectural role in assembling the specific DNA–protein complex for DNA replication, regulation of transcription, and condensation of DNA into chromatin.

Two early AFM studies investigated the DNA bending induced by *E. coli* RNAP (Rees *et al*., 1993) and bacteriophage λ Cro, a small transcription regulatory protein (Erie *et al*., 1994). In the AFM study of the RNAP, the DNA appeared bent in open promoter complexes containing RNAP bound to the promoter, and more severely bent in elongation complexes in which RNAP has synthesized a 15-nucleotide transcript (Rees *et al*., 1993). The different bent conformations of DNA induced by RNAP were proposed to be the characteristics of polymerase transiting from the open promoter complexes to the elongation complexes (Rees *et al*., 1993). In the Cro study, Erie *et al*. analyzed the fundamental roles of protein-induced DNA bending at specific sites as well as at nonspecific sites (Erie *et al*., 1994). Protein-induced bending at nonspecific sites was observed and it was suggested to be important for protein in searching for specific sites and increasing specificity on the target sites (Erie *et al*., 1994). AFM has also been used to study specific and nonspecific photolyase–DNA complexes (van Noort *et al*., 1999). Photolyase is an enzyme that binds to UV-induced thymidine dimers and reverses the cross-linking of adjacent pyrimidines by using the energy of visible light. Contrary to Cro–DNA complexes, nonspecific photolysase–DNA complexes show no significant bending but increased rigidity compared with naked DNA, whereas specific complexes show average DNA bending of 36° and higher flexibility (van Noort *et al*., 1999).

It is worth pointing out that though other DNA bending assays, such as gel mobility, yield a single or average bend angle, AFM provides the spatial distribution of bending along the DNA and dynamic bending histograms of DNA–protein assemblies bound at the same location; that is, the full distribution of angles is observed. Knowledge of the full distribution of bend angles can provide unique insight into the mechanism of action by proteins, such as in the case of MutS (Wang

et al., 2003). The family of MutS proteins initiates DNA mismatch repair (MMR) by the recognition of base–base mismatches and insertion or deletion loops. To gain insight into the mechanism by which MutS discriminates between mismatch and homoduplex DNA, protein-induced DNA bending at specific and nonspecific MutS–DNA complexes has been studied by AFM (Wang *et al*., 2003; Figure 2.7A). Interestingly, MutS–DNA complexes exhibit a single population of conformations, in which the DNA is bent at homoduplex sites, but two populations of conformations, bent and unbent, at mismatch sites (Figure 2.7B). These results suggest that the specific recognition complex is one in which the DNA is unbent. Combining these results with existing biochemical and crystallographic data led to the proposal that MutS (i) binds to DNA nonspecifically and bends it in search of a mismatch; (ii) on specific recognition of a mismatch, undergoes a conformational change to an initial recognition complex in which the DNA is kinked, with interactions similar to those in the published crystal structures; and (iii) finally undergoes a further conformational change to the ultimate recognition complex in which the DNA is unbent (Wang *et al*., 2003). The results from this study provide one structural explanation that can contribute to the further understanding of how MutS achieves high MMR specificity.

Interestingly, AFM imaging has shown that simultaneous binding of two cellular transcription factors, nuclear factor I (NFI) and octamer-binding protein (Oct-1), can induce a collective bend in DNA, when bound to the transcription origin (Mysiak *et al*., 2004a,b). Mysiak *et al*. observed that NFI induced a 60° bend in the origin DNA, whereas Oct-1 induced a 42° bend. Simultaneous binding of NFI and Oct-1 induces an 82° bend. It was suggested that this collective DNA bending can lead to a synergistic enhancement of DNA replication (Mysiak *et al*., 2004b).

DNA bending induced by other proteins, such as EcoRI and adenine N6 DNA methyltransferases, has also been observed using AFM (Garcia *et al*., 1996; Allan *et al*., 1999; van Noort *et al*., 1999; Mysiak *et al*., 2004a). In addition to DNA bending, other DNA distortions, such as DNA wrapping, have been observed for protein involved in transcription, DNA repair, replication initiation, and chromatin remodeling. These proteins include RNAP, UvrB, human replication protein A (RPA), chromatin remodeling factor CSB, DNA gyrase, histone protein, and DNA replication ORC (Rivetti *et al*., 1999; Verhoeven *et al*., 2001; Lysetska *et al*., 2002; Kepert *et al*., 2003; Rivetti *et al*., 2003; Gaczynska *et al*., 2004; Heddle *et al*., 2004). In AFM images, DNA wrapping around a protein is observed as a reduced DNA contour length when comparing DNA length from DNA–protein complexes with free DNA.

AFM has also been used to visualize the unwinding of duplex RNA by DbpA, which is a DEAD box helicase (Henn *et al*., 2001). The DEAD box protein family catalyzes the hydrolysis of ATP in the presence of RNA. From AFM imaging, Henn *et al*. (2001) observed that DbpA was bound to the end of RNA molecule with a ssRNA overhang, indicating that DbpA requires an ssRNA or moderate fork junction for binding before performing the unwinding activity. The unwinding of

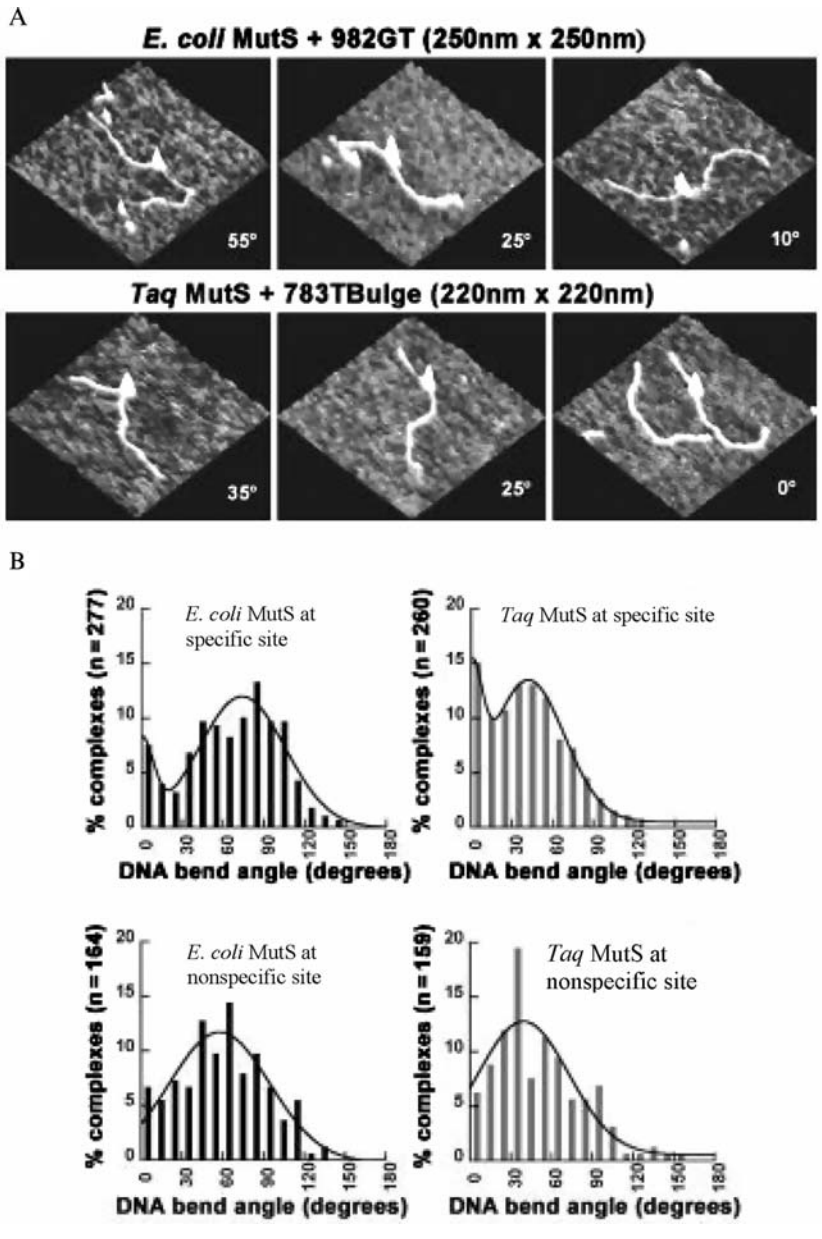

Figure 2.7. Using atomic force microscopy (AFM) imaging to study the protein-induced DNA bending. (A) AFM surface plots of *E. coli* MutS bound to a G–T mismatch and *Taq* MutS bound to a 1T-bulge. MutS-induced DNA bend angles are shown on each image. (B) Histograms of DNA bend angles induced by *E. coli* and *Taq* MutS bound to mismatch (specific complexes, *upper panels*) and homoduplex (nonspecific complexes, *lower panels*) sites. The images and the plots are reproduced from Wang *et al.* (2003) with permission.

duplex RNA was observed as ATP simulated formation of Y-shaped intermediate, representing strand separation.

2.3.5. Characterization of Collective Actions of Protein Assemblies at Multiple Sites on DNA

Although some reactions on DNA are carried out by a single protein at one specific site, many reactions involve multiple proteins interacting with multiple sites that span long distances along the DNA. This section highlights the applications of AFM to study the cooperative protein binding to DNA, protein-mediated DNA condensation, DNA looping, and end joining.

2.3.5.1. Cooperative DNA Binding by Proteins

RecA is a classic allosterically regulated enzyme, and ATP binding leads to a dramatic increase in DNA-binding affinity and a cooperative assembly of RecA subunits to form a helical nucleoprotein filament. RecA filaments on DNA play an important role in promoting recombination between two DNA strands and regulating the SOS response in bacteria (McGrew and Knight, 2003). AFM imaging of RecA filaments using carbon nanotube probes revealed a 10-nm pitch of RecA–dsDNA complex (Umemura *et al*., 2001), which is consistent with the observation from EM. This study shows that high-resolution AFM images of RecA filaments can provide useful information for constructing a 3D structural model for a RecA–DNA filament. Recently, examination of the formation of RecA–dsDNA complex as a function of time using AFM provided insight into the mechanism of assembly of the RecA filament (Sattin and Goh, 2004). In the study carried by Sattin *et al*., RecA was incubated with nicked plasmid DNA in the presence of ATPγS (adenosine-5′ (γ-thio)-triphosphate), and aliquots of reaction were taken at different time points and deposited on mica for AFM imaging. AFM imaging revealed that extensive polymerization of the RecA along DNA did not happen until after 15 min, and at later time, the RecA coverage of plasmid DNA was continuous, with no instances of a plasmid with more than one continuous stretch of RecA filament (Figure 2.8A–C). These findings suggested that the nucleation step of RecA binding to DNA is very unfavorable, and it is slow, whereas the polymerization step is fast. In addition, AFM imaging also showed that homologs of RecA, such as archaeal RadA and *Saccharomyces cerevisiae* Dmc1, also form protein filaments on DNA (Seitz *et al*., 1998; Chang *et al*., 2005).

MutL and its homologs are essential components of postreplicative DNA MMR systems (Modrich and Lahue, 1996; Buermeyer *et al*., 1999; Kolodner and Marsischky, 1999). In addition, MutL and its homologs also participate in a variety of other DNA transactions, such as cell-cycle checkpoint control, apoptosis, and regulation of homologous and homeologous recombination (Buermeyer *et al*., 1999; Bellacosa, 2001). The detailed knowledge of DNA-binding mechanism of MutL homologs is a perquisite to understanding their roles in different DNA

transactions. Using AFM, it was demonstrated that yeast MutL homolog, MLH1–PMS1, can form cooperative protein assemblies on either one or two strands of DNA (Figure 2.8D–F), suggesting that it has at least one independent DNA-binding site on each of its subunits (Hall *et al*., 2001; Drotschmann *et al*., 2002; Hall *et al*., 2003). Unlike RecA filaments, there were multiple MLH1–PMS1 protein tracts on one M13 plasmid. These data suggest that for MLH1–PMS1, although the nucleation event is significantly less favorable than the polymerization, it is not so unfavorable as in the case of RecA for which only a single protein tract is seen on each plasmid.

2.3.5.2. Protein-Mediated DNA Condensation

Genomic DNA needs to be packaged to fit into its cellular compartments (Sato *et al*., 1999; Dame *et al*., 2000; Brewer *et al*., 2003; Ceci *et al*., 2004; Friddle *et al*., 2004). Mammals and the budding yeast package mtDNA in compact globular

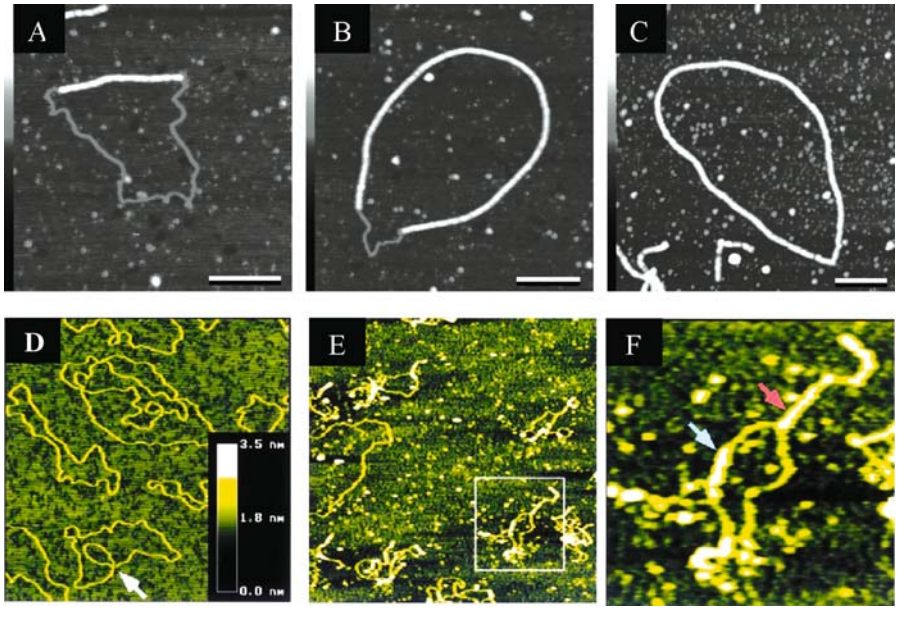

Figure 2.8. Using atomic force microscopy (AFM) imaging to study the cooperative binding of protein on dsDNA. (A–C) Typical RecA–DNA complexes observed at different incubation times at 37°C: (A) After 30 min—∼38% coverage of DNA by RecA; (B) 45 min—∼88% coverage; and (C) 60 min—DNA fully coated by RecA. The images are reproduced from Sattin and Goh (2004) with permission. (D–F) Cooperative binding of yeast MLH1–PMS1 heterodimer to dsDNA: (D) M13mp2 RFI DNA alone. (E) M13 RFI DNA in the presence of MLH1–PMS1. The scan size is 1500 nm for (D) and (E). (F) Zoomed view of the boxed region in (E). The light blue arrow indicates a tract of cooperatively bound MLH1–PMS1 associated with a single dsDNA region. The red arrow indicates a tract of cooperatively bound MLH1–PMS1 associated with two dsDNA regions. The images are reproduced from Hall *et al*. (2001) with permission.

structures are similar to a bacterial nucleoid, and its structure is distinctly different from the packaging of DNA into chromatin in the cell nucleus, which involves wrapping of the DNA around histone proteins. DNA compaction involves collective efforts of multiple copies of proteins over a large distance at discrete sites. Compaction of linear DNA by yeast mitochondrial protein Abf2p was investigated by AFM as a function of protein concentration (Brewer *et al*., 2003). At low protein concentrations, DNA bending and compaction were observed, whereas at high protein concentrations, round compact objects were observed (Brewer *et al*., 2003). Based on these observations, Friddle *et al*. (2004) suggested that Abf2p compacts DNA by introducing sharp bends into the DNA backbone. On the other hand, for *E. coli* H-NS protein, DNA bridging mediated by H-NS and highly compacted DNA was observed with co-occurrence of relative high features on the DNA. These data suggest that compaction of DNA is mediated by DNA bridging and extensive oligomerization of bound H-NS molecules (Dame *et al*., 2000). In addition, at higher ratio of H-NS–DNA, the complexes have a rod-like appearance, indicating high level of condensation through network formation. The protein RdgC, which was suggested to play a role in replication and recombination, has also been implicated in promoting DNA condensation (Tessmer *et al*., 2005). For the protein RdgC, both RdgC-induced DNA bending and protein–protein mediated strongly interwound dense DNA structures were observed in AFM images (Tessmer *et al*., 2005).

2.3.5.3. Proteins Bind to Multiple Sites on DNA Leading to DNA Looping and End Joining

Two pathways can lead to DNA looping. First, protein–protein complexes can bind concurrently to two sites forming a loop with fixed size. Second, energy-dependent translocation of one or more subunits along the DNA relative to the other subunit can result in DNA looping with loop size not fixed. Examples are DNA looping by restriction enzymes and during transcription activation process (Rippe *et al*., 1997; Halford *et al*., 2004). The restriction enzymes that interact with two sites on the DNA include all the endonucleases from the Type I and III restriction–modification systems and many of the type II restriction enzymes (Halford *et al*., 2004). Even though people are more familiar with the restriction enzymes that act at a single specific site, these enzymes are indeed a minority compared with those needing two sites. DNA looping on linearized plasmid, through dimerization of proteins bound to two binding sites, has been observed with a type IA restriction enzyme, EcoKI (Berge *et al*., 2000). It was suggested that the requirement for interaction with two sites for cleavage may increase specificity and prevent the promiscuous cleavage by restriction endonucleases (Halford *et al*., 2004).

Transcriptional enhancers are *cis*-acting DNA elements that are binding sites for regulatory proteins and function at large distances from promoter elements to stimulate transcription (Xu and Hoover, 2001). Enhancer-like elements have been

discovered in eukaryotes and in a wide variety of bacteria. The regulatory proteins that bind to enhancers must contact RNAP to activate transcription. Interactions between enhancer-binding proteins and RNAP can occur by either DNA looping or tracking of the enhancer-binding protein along the DNA. AFM has shown that contact of an activator protein NtrC and sigma (54)-RNAP holoenzyme is mediated by DNA looping (Rippe *et al*., 1997).

In an earlier section, we mentioned the importance of the correct processing of DNA ends to the integrity of the genome. DNA-PK plays important roles in DNA double-strand break repair and immunoglobulin gene rearrangement. The DNA-PK holoenzyme is composed of three polypeptide subunits: The DNA-binding Ku70/Ku86 heterodimer and a catalytic subunit (DNA-PKcs). AFM has been used to visualize the interaction of Ku and DNA-PK with DNA (Cary *et al*., 1997). Ku-mediated DNA looping was observed, and the loop formation was independent of DNA sequence and of the presence of DNA-PKcs (Cary *et al*., 1997). To differentiate whether Ku tethered DNA ends through self-association of the DNA-bound proteins or a capacity for the complex to bind two DNA ends simultaneously, gel filtration of Ku in the absence and the presence of DNA was conducted. Gel filtration showed no evidence of self-association of two Ku70/Ku86 in the absence of DNA but association of two Ku70/Ku86 in the presence of DNA. These observations suggested that Ku binding at DNA double-strand breaks leads to Ku self-association and a physical tethering of the broken DNA strands. AFM imaging directly supports the notion that the Ku70/Ku86 heterodimer is capable of holding or tethering broken ends in place through self-association to ensure physical proximity of DNA ends for correct repair. It is worth mentioning that AFM imaging also demonstrated that telomere repeat binding factor, TRF2, also uses DNA-dependent multimerization to form DNA loops (Yoshimura *et al*., 2004). It was suggested that this TRF protein-mediated DNA loop might be an important intermediate structure for protection of chromosome ends.

Previously, we discussed that AFM imaging has resolved the globular and arm domain of human Rad50–Mre11 complex and the study of its end-binding specificity (de Jager *et al*., 2001). AFM imaging has also demonstrated that Rad50–Mre11 formed large oligomeric protein complexes at DNA ends, and the arms protruded from the DNA (de Jager *et al*., 2001). Based on these observations, it is suggested that Rad50–Mre11 oligomers accumulate at broken DNA ends and keep the ends in close proximity by interaction of the end-bound Rad50–Mre11 oligomers through interaction of their arm domains (de Jager *et al*., 2001, 2002).

2.3.6. Characterization of Protein Fibers

Most of the proteins we have discussed so far are globular proteins, in which the polypeptide chain folds into a compact shape like a ball with an irregular surface. Fibrous proteins form the cytoskeleton inside the cell. They are also a main component of the gel-like extracellular matrix that is responsible for tissue strength and resilience and promoting cell growth and differentiation. In addition,

blood clots, which prevent the loss of blood after injury, mainly consist of fibrin fibers attached to platelets. Understanding the structure and mechanical properties of protein fibers can help us understand the normal function of these fibrous proteins and various disease states that are caused by the defects in the polymerization and degradation of fibrous proteins. The ability of AFM to image in air and liquids, and to manipulate samples makes it a unique tool for studying fibrous proteins.

Recently, Guthold *et al*. demonstrated the ability of AFM to visualize and mechanically manipulate individual fibrin fibers, which are the key structural components of blood clots. Using lateral force manipulation (see Section 2.2.6 and Figure 2.9), Guthold *et al*. determined the rupture force, F_R, as a function of diameter of fibrin fiber, D. They found that the rupture force increased with increasing diameter as $F_R \sim D^{1.30\pm0.06}$. This observation suggested that the molecule density (ρ) of fibrin fiber varies as $\rho(D) \sim D^{0.7}$, which means that thinner fibers are denser than thicker fibers. Future comparison studies of the mechanical properties of fibrin fibers formed from precursors obtained from healthy people and people with blood clotting disorder will further our understanding of the disease state.

Abnormal formation of protein fibril by aggregation of normally soluble proteins can also cause various diseases. The amyloid fibril, which has characteristic filamentous structures, is involved in a range of human diseases, such as Alzheimer's disease, type II diabetes, Parkinson's diseases, and Huntington's disease. *In vitro*, the polymerization of many amyloids can be initiated by the formation of a seeding nucleus or protofibril followed by the assembly of soluble protein assemblies with these nuclei to form amyloid fibers (see Figure 2.10A). Therapeutic intervention for these diseases depends on detailed understanding of the molecular mechanisms governing fibril assembly. AFM can recapitulate the fibril morphologies that have been shown by EM (Goldsbury *et al*., 1999). For example, for amylin fibril, which is the protein component of the pancreatic amyloid deposits in type II diabetes, AFM imaging revealed a distinct 25-nm crossover repeat that is consistent with the observation from EM (Goldsbury *et al*., 1999). More importantly, time-lapse AFM imaging in liquids has been used to continuously monitor the growth, directionality, and changes in the morphology of individual fibrils (see Figure 2.10B; Goldsbury *et al*., 1999, 2001; Stolz *et al*., 2000). This time-lapse AFM imaging in liquids showed that growth of the amylin and β-amyloid protofibrils was bidirectional (see Figure 2.10B; Goldsbury *et al*., 1999; Blackley *et al*., 2000). In addition, the outgrowth of protofibrils from a common amyloid core is also observed (Blackley *et al*., 2000).

AFM has been used to look for the factors, possibly an abnormal metabolite, that can dramatically accelerate the amyloidogenesis, which might explain why wild-type protein only misfolds in a small percentage of human population (Zhang *et al*., 2004). Using AFM, Zhang *et al*. reported that in the absence of ketoaldehyde or its aldol product Aβ amyloidogenesis was not observed whereas in their presence spherical assemblies appeared (Zhang *et al*., 2004). On addition of fibrillar seeds, the spherical aggregates are rapidly converted into fibril, whereas without the ketoaldehyde, the process was much slower.

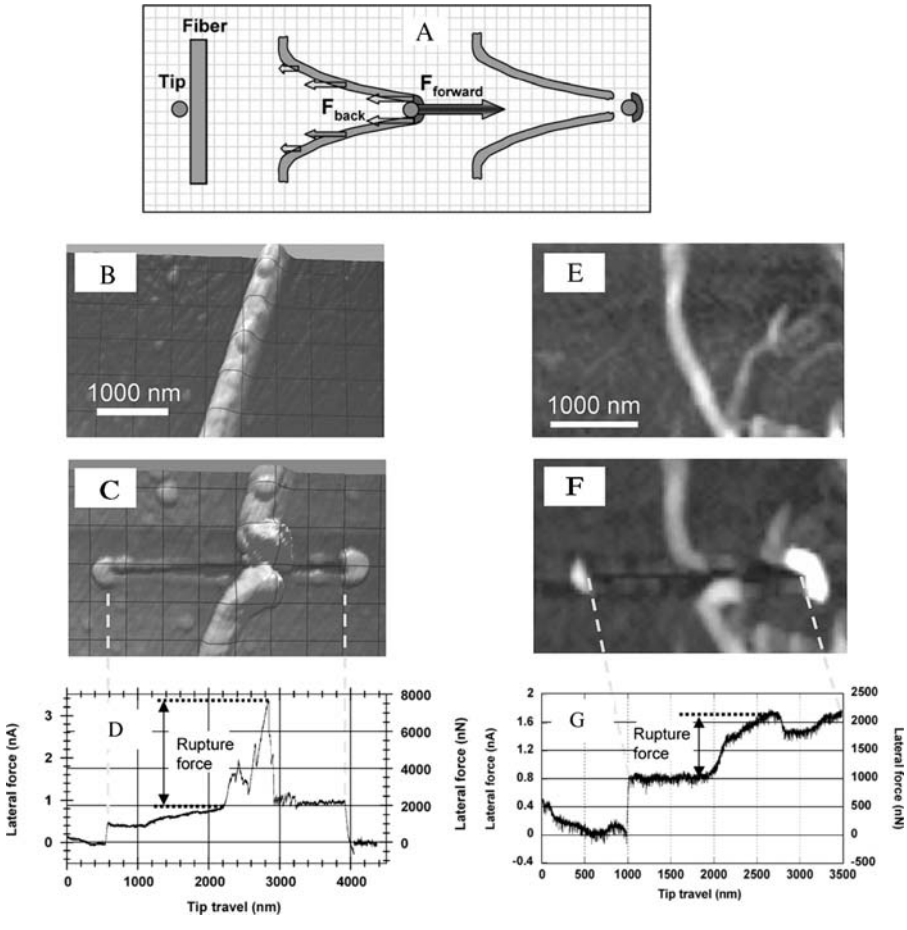

Figure 2.9. Lateral force manipulation of fibrin fiber. (A) Schematics of a fiber manipulation. The tip contacts the fiber, and stretches it until it ruptures. During manipulation, two main forces (a force pair) act on the fiber segment that ruptures (dark red): the backward distributed frictional force and the forward applied tip force. Those two forces balance each other and cause the fiber to deform and to eventually rupture. (B–G) atomic force microscopy (AFM) images of two fibrin fibers before and after being ruptured by the AFM tip, and corresponding lateral force versus tip travel during this manipulation. Dotted vertical lines between C and D, and F and G align scratched trace in images after manipulation with tip travel trace. Images and diagrams are reproduced from Guthold *et al*. (2004) with permission.

AFM has also been used in search for the fibril elongation inhibitors (Li *et al*., 2004). For example, AFM has been used to monitor the dopamine-induced dissolution of single α-synuclein fibril immobilized on mica in aqueous solution (Li *et al*., 2004). Dopamine is a key neuromuscular neurotransmitter. This study showed that in the presence of dopamine, the initial fibril was significantly disassembled in 1 h and is completely dissociated in 2 h (see Figure 2.10C). Even though dopamine is

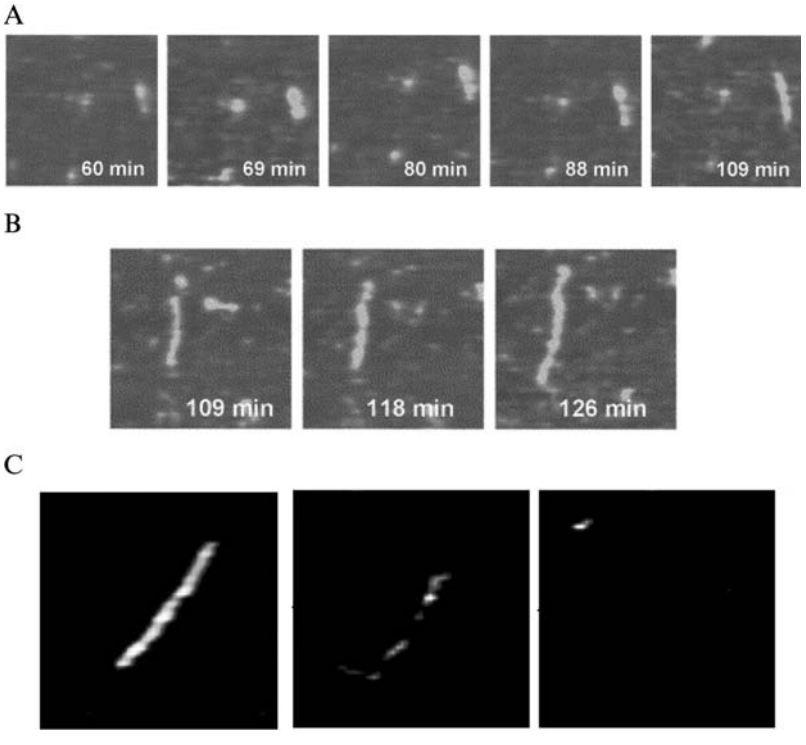

Figure 2.10. Using atomic force microscopy (AFM) to study the structure and assembly of amyloid fibrils. (A) The formation of protofibrils through single aggregate of β-amyloid and subsequent elongation by the addition of further aggregate units of β-amyloid. (B) The bidirectional elongation of a β-amyloid protofibril by the addition of aggregate units of β-amyloid. The images from (A) and (B) panels are reproduced from Blackley *et al*. (2000) with permission. (C) Disassembly of a single fibril of α-synuclein monitored by time-lapse AFM in liquids. Dopamine was added to a solution of preformed α-synuclein fibrils and an aliquot was deposited on mica. Panels from left to right show a specific fibril 0, 1, and 2 h after adding dopamine. The images are reproduced from Li *et al*. (2004) with permission.

not suitable for use as a drug, future AFM studies will open new possibilities for therapeutic intervention of disease caused by protein aggregations.

2.3.7. Following Biological Processes Using Imaging in Liquids

Applications of AFM imaging in liquids to study membrane proteins, fibril formation, and degradation have been mentioned in the earlier sections. This section discusses more applications of imaging in liquids. The biomolecular assemblies and interactions in biological pathways take place in a timed fashion in the cell. Time-lapse AFM imaging in liquids can be used to follow these processes under near-physiological conditions. For example, the DNA-directed synthesis

of RNA by *E. coli* RNAP has been observed using AFM solution imaging (Argaman *et al*., 1997). In addition, the degradation of DNA by the nuclease DNase I was followed by oscillating mode AFM in solution in the presence of nickel ions (Bezanilla *et al*., 1994). Many quantitative dynamic properties of these processes can be obtained using time-lapse AFM in solution. For example, the rate of the diffusion of *E. coli* RNAP on the DNA was measured using time-lapse AFM. The rate was found to be 1.5 nucleotides per second, which is about three times slower than the speed in solution. This was expected because the surface could hamper the diffusion (Guthold *et al*., 1999b). Finally, very detailed enzyme kinetics of phospholipase A_2 has been analyzed using AFM imaging in liquids (Balashev *et al*., 2001).

In addition to the earlier quantitative assays, it is also possible to directly qualitatively correlate structural conformations and functional states of individual biomolecular assemblies using time-lapse AFM imaging (Stolz *et al*., 2000). For example, the conformational change of nuclear pore complexes modulated by ATP, calcium, and carbon dioxide have been studied using time-lapse AFM (Rakowska *et al*., 1998; Stoffler *et al*., 1999; Oberleithner *et al*., 2000). These studies disclosed that ATP and calcium induce the pore contraction and facilitate the transportation of macromolecules between the nucleus and the cytosol, whereas carbon dioxide induces pore collapse and functions to isolate the nucleus. Although time-lapse AFM has powerful capabilities, limitations on this dynamic approach also exist. First, the resolution limitation due to the noise in time-lapse imaging in liquids limits its use for studying small biomolecular assemblies. Second, limitations of scanning speed of commercial AFM instruments make it impossible to observe many fast biological processes (Ando *et al*., 2001); however, this limitation is overcome with recent advances in instrumentation.

2.3.8. AFM as a Tool for Proteomics

The accelerating determination of genome sequences and their interpretation (genomics) has brought with it one of the most daunting challenges to modern biological sciences, that is, the concomitant determination of the structure, function, protein–protein interactions, and expression of all the corresponding proteins that are encoded by the genomic DNA. The rapid advance of the field of proteomics depends on traditional biochemical techniques and new innovations. Microarrays have been established as a standard for parallel screening of the nucleic acids profiles. Recently, exciting new technology based on AFM has emerged which has the potential to be used in high-throughput screening of protein–protein interactions (Lynch *et al*., 2004). A new instrument called the NanoArrayer can mechanically mediate direct deposition of materials on surface with spot size several hundred nanometers to 2 μm in diameter. After adding the second protein, the detection of protein–protein interactions on the protein array can be carried out by fluorescence microscopy (in case the second protein added is fluorescent) or monitoring the height increase by AFM imaging.

2.4. CONCLUDING REMARKS

AFM is a versatile tool, which allows us to investigate the protein–protein interactions from different perspectives. In the past several years, there is an exciting trend of designing new diversified AFM instruments. Besides the Nanomanipulator and Nanoarrayer mentioned earlier, people have combined AFM with fluorescence microscope (Vickery and Dunn, 2001; Kassies *et al*., 2005). These emerging new instruments will continue to expand our vision and reach into the realm of protein–protein complexes at the molecular level.

ACKNOWLEDGMENTS

We thank Drs Thomas A. Kunkel and Bennett Van Houten for helpful comments on the manuscript. This work was supported in part by National Institutes of Health grants GM54136 and the American Cancer Society (to D.A.E.).

REFERENCES

Abels, J. A., Moreno-Herrero, F., van der Heijden, T., Dekker, C., and Dekker, N. H. (2005). Single-molecule measurements of the persistence length of double-stranded RNA. *Biophys J* 88:2737–2744.

Abu-Lail, N. I. and Camesano, T. A. (2003). Polysaccharide properties probed with atomic force microscopy. *J Microsc* 212:217–238.

Allan, B. W., Garcia, R., Maegley, K., Mort, J., Wong, D., Lindstrom, W., Beechem, J. M., and Reich, N. O. (1999). DNA bending by EcoRI DNA methyltransferase accelerates base flipping but compromises specificity. *J Biol Chem* 274:19269–19275.

Allison, D. P., Kerper, P. S., Doktycz, M. J., Spain, J. A., Modrich, P., Larimer, F. W., Thundat, T., and Warmack, R. J. (1996). Direct atomic force microscope imaging of EcoRI endonuclease site specifically bound to plasmid DNA molecules. *Proc Natl Acad Sci USA* 93:8826–8829.

Ando, T., Kodera, N., Takai, E., Maruyama, D., Saito, K., and Toda, A. (2001). A high-speed atomic force microscope for studying biological macromolecules. *Proc Natl Acad Sci USA* 98:12468–12472.

Argaman, M., Golan, R., Thomson, N. H., and Hansma, H. G. (1997). Phase imaging of moving DNA molecules and DNA molecules replicated in the atomic force microscope. *Nucleic Acids Res* 25:4379–4384.

Balashev, K., Jensen, T. R., Kjaer, K. and Bjornholm, T. (2001). Novel methods for studying lipids and lipases and their mutual interaction at interfaces. Part I. Atomic force microscopy. *Biochimie* 83:387–397.

Bao, K. K., Wang, H., Miller, J. K., Erie, D. A., Skalka, A. M., and Wong, I. (2003). Functional oligomeric state of avian sarcoma virus integrase. *J Biol Chem* 278:1323–1327.

Bellacosa, A. (2001). Functional interactions and signaling properties of mammalian DNA mismatch repair proteins. *Cell Death Differ* 8:1076–1092.

Berge, T., Ellis, D. J., Dryden, D. T., Edwardson, J. M., and Henderson, R. M. (2000). Translocation-independent dimerization of the EcoKI endonuclease visualized by atomic force microscopy. *Biophys J* 79:479–484.

Bezanilla, M., Drake, B., Nudler, E., Kashlev, M., Hansma, P. K., and Hansma, H. G. (1994). Motion and enzymatic degradation of DNA in the atomic force microscope. *Biophys J* 67:2454–2459.

Binnig, G., Quate, C. F., and Gerber, C. (1986). Atomic force microscope. *Phys Rev Lett* 56:930–933.

Blackley, H. K., Sanders, G. H., Davies, M. C., Roberts, C. J., Tendler, S. J., and Wilkinson, M. J. (2000). In-situ atomic force microscopy study of beta-amyloid fibrillization. *J Mol Biol* 298:833–840.

Bockelmann, U. (2004). Single-molecule manipulation of nucleic acids. *Curr Opin Struct Biol* 14: 368–373.

Bonin, M., Oberstrass, J., Lukacs, N., Ewert, K., Oesterschulze, E., Kassing, R., and Nellen, W. (2000). Determination of preferential binding sites for anti-dsRNA antibodies on double-stranded RNA by scanning force microscopy. *RNA* 6:563–570.

Brewer, L. R., Friddle, R., Noy, A., Baldwin, E., Martin, S. S., Corzett, M., Balhorn, R., and Baskin, R. J. (2003). Packaging of single DNA molecules by the yeast mitochondrial protein Abf2p. *Biophys J* 85:2519–2524.

Bucior, I. and Burger, M. M. (2004). Carbohydrate–carbohydrate interactions in cell recognition. *Curr Opin Struct Biol* 14:631–637.

Buermeyer, A. B., Deschenes, S. M., Baker, S. M., and Liskay, R. M. (1999). Mammalian DNA mismatch repair. *Annu Rev Genet* 33:533–564.

Bustamante, C., Macosko, J. C., and Wuite, G. J. (2000). Grabbing the cat by the tail: manipulating molecules one by one. *Nat Rev Mol Cell Biol* 1:130–136.

Bustamante, C. and Rivetti, C. (1996). Visualizing protein-nucleic acid interactions on a large scale with the scanning force microscope. *Annu Rev Biophys Biomol Struct* 25:395–429.

Bustamante, C., Zuccheri, G., Leuba, S. H., Yang, G., and Samori, B. (1997). Visualization and analysis of chromatin by scanning force microscopy. *Methods* 12:73–83.

Carrion-Vazquez, M., Oberhauser, A. F., Fowler, S. B., Marszalek, P. E., Broedel, S. E., Clarke, J., and Fernandez, J. M. (1999). Mechanical and chemical unfolding of a single protein: a comparison. *Proc Natl Acad Sci USA* 96:3694–3699.

Cary, R. B., Peterson, S. R., Wang, J., Bear, D. G., Bradbury, E. M., and Chen, D. J. (1997). DNA looping by Ku and the DNA-dependent protein kinase. *Proc Natl Acad Sci USA* 94:4267–4272.

Ceci, P., Cellai, S., Falvo, E., Rivetti, C., Rossi, G. L., and Chiancone, E. (2004). DNA condensation and self-aggregation of *Escherichia coli* Dps are coupled phenomena related to the properties of the N-terminus. *Nucleic Acids Res* 32:5935–5944.

Chang, Y. C., Lo, Y. H., Lee, M. H., Leng, C. H., Hu, S. M., Chang, C. S., and Wang, T. F. (2005). Molecular visualization of the yeast Dmc1 protein ring and Dmc1-ssDNA nucleoprotein complex. *Biochemistry* 44:6052–6058.

Chen, L., Haushalter, K. A., Lieber, C. M., and Verdine, G. L. (2002). Direct visualization of a DNA glycosylase searching for damage. *Chem Biol* 9:345–350.

Chilkoti, A., Boland, T., Ratner, B. D., and Stayton, P. S. (1995). The relationship between ligand-binding thermodynamics and protein-ligand interaction forces measured by atomic force microscopy. *Biophys J* 69:2125–2130.

Clausen-Schaumann, H., Seitz, M., Krautbauer, R., and Gaub, H. E. (2000). Force spectroscopy with single bio-molecules. *Curr Opin Chem Biol* 4:524–530.

Colton, R. J., Engel, A., Frommer, J. E., Gaub, H. E., Gewirth, A. A., Guckenberger, R., Rabe, J., Heckl, W. M., and Parkinson, B. (1998). *Procedures in Scanning Probe Microscopies*. John Wiley & Sons, London.

Conroy, M. J., Jamieson, S. J., Blakey, D., Kaufmann, T., Engel, A., Fotiadis, D., Merrick, M., and Bullough, P. A. (2004). Electron and atomic force microscopy of the trimeric ammonium transporter AmtB. *EMBO Rep* 5:1153–1158.

Czajkowsky, D. M. and Shao, Z. (2003). Inhibition of protein adsorption to muscovite mica by monovalent cations. *J Microsc* 211:1–7.

Dame, R. T., Wyman, C., and Goosen, N. (2000). H-NS mediated compaction of DNA visualised by atomic force microscopy. *Nucleic Acids Res* 28:3504–3510.

Dammer, U., Popescu, O., Wagner, P., Anselmetti, D., Guntherodt, H. J., and Misevic, G. N. (1995). Binding strength between cell adhesion proteoglycans measured by atomic force microscopy. *Science* 267:1173–1175.

de Jager, M., van Noort, J., van Gent, D. C., Dekker, C., Kanaar, R., and Wyman, C. (2001). Human Rad50/Mre11 is a flexible complex that can tether DNA ends. *Mol Cell* 8:1129–1135.

de Jager, M., Wyman, C., van Gent, D. C., and Kanaar, R. (2002). DNA end-binding specificity of human Rad50/Mre11 is influenced by ATP. *Nucleic Acids Res* 30:4425–4431.

Dickerson, R. E. (1998). DNA bending: the prevalence of kinkiness and the virtues of normality. *Nucleic Acids Res* 26:1906–1926.

Drake, B., Prater, C. B., Weisenhorn, A. L., Gould, S. A., Albrecht, T. R., Quate, C. F., Cannell, D. S., Hansma, H. G., and Hansma, P. K. (1989). Imaging crystals, polymers, and processes in water with the atomic force microscope. *Science* 243:1586–1589.

Drotschmann, K., Hall, M. C., Shcherbakova, P. V., Wang, H., Erie, D. A., Brownewell, F. R., Kool, E. T., and Kunkel, T. A. (2002). DNA binding properties of the yeast Msh2-Msh6 and Mlh1–Pms1 heterodimers. *Biol Chem* 383:969–975.

Edwardson, J. M. and Henderson, R. M. (2004). Atomic force microscopy and drug discovery. *Drug Discov Today* 9:64–71.

Engel, A. and Muller, D. J. (2000). Observing single biomolecules at work with the atomic force microscope. *Nat Struct Biol* 7:715–718.

Erie, D. A., Yang, G., Schultz, H. C., and Bustamante, C. (1994). DNA bending by Cro protein in specific and nonspecific complexes: implications for protein site recognition and specificity. *Science* 266:1562–1566.

Fisher, T. E., Marszalek, P. E., and Fernandez, J. M. (2000). Stretching single molecules into novel conformations using the atomic force microscope. *Nat Struct Biol* 7:719–724.

Florin, E. L., Moy, V. T., and Gaub, H. E. (1994). Adhesion forces between individual ligand-receptor pairs. *Science* 264:415–417.

Fotiadis, D. and Engel, A. (2004). High-resolution imaging of bacteriorhodopsin by atomic force microscopy. *Methods Mol Biol* 242:291–303.

Friddle, R. W., Klare, J. E., Martin, S. S., Corzett, M., Balhorn, R., Baldwin, E. P., Baskin, R. J., and Noy, A. (2004). Mechanism of DNA compaction by yeast mitochondrial protein Abf2p. *Biophys J* 86:1632–1639.

Fritzsche, W., Takac, L., and Henderson, E. (1997). Application of atomic force microscopy to visualization of DNA, chromatin, and chromosomes. *Crit Rev Eukaryot Gene Expr* 7:231–240.

Gaczynska, M., Osmulski, P. A., Jiang, Y., Lee, J. K., Bermudez, V., and Hurwitz, J. (2004). Atomic force microscopic analysis of the binding of the *Schizosaccharomyces pombe* origin recognition complex and the spOrc4 protein with origin DNA. *Proc Natl Acad Sci USA* 101:17952–17957.

Garcia, R. A., Bustamante, C. J., and Reich, N. O. (1996). Sequence-specific recognition of cytosine C5 and adenine N6 DNA methyltransferases requires different deformations of DNA. *Proc Natl Acad Sci USA* 93:7618–7622.

Gettens, R. T., Bai, Z., and Gilbert, J. L. (2005). Quantification of the kinetics and thermodynamics of protein adsorption using atomic force microscopy. *J Biomed Mater Res A* 72:246–257.

Goldsbury, C., Aebi, U., and Frey, P. (2001). Visualizing the growth of Alzheimer's A beta amyloid-like fibrils. *Trends Mol Med* 7:582.

Goldsbury, C., Kistler, J., Aebi, U., Arvinte, T., and Cooper, G. J. (1999). Watching amyloid fibrils grow by time-lapse atomic force microscopy. *J Mol Biol* 285:33–39.

Guthold, M., Falvo, M., Matthews, W. G., Paulson, S., Mullin, J., Lord, S., Erie, D., Washburn, S., Superfine, R., Brooks, F. P. Jr., and Taylor, R. M. II (1999a). Investigation and modification of molecular structures with the nanoManipulator. *J Mol Graph Model* 17:187–197.

Guthold, M., Falvo, M., Matthews, W. G., Paulson, S., Mullin, J., Lord, S., Erie, D., Washburn, S., Superfine, R., Brooks, F. P., and Taylor, R. M. (2000). Investigation and modification of molecular structures with the nanoManipulator. *J Mol Graph Model* 17:187–197.

Guthold, M., Liu, W., Stephens, B., Lord, S. T., Hantgan, R. R., Erie, D. A., Taylor, R. M. Jr., and Superfine, R. (2004). Visualization and mechanical manipulations of individual fibrin fibers suggest that fiber cross section has fractal dimension 1.3. *Biophys J* 87:4226–4236.

Guthold, M., Zhu, X., Rivetti, C., Yang, G., Thomson, N. H., Kasas, S., Hansma, H. G., Smith, B., Hansma, P. K., and Bustamante, C. (1999b). Direct observation of one-dimensional diffusion and transcription by *Escherichia coli* RNA polymerase. *Biophys J* 77:2284–2294.

Gutsmann, T., Fantner, G. E., Kindt, J. H., Venturoni, M., Danielsen, S., and Hansma, P. K. (2004). Force spectroscopy of collagen fibers to investigate their mechanical properties and structural organization. *Biophys J* 86:3186–3193.

Hafner, J. H., Cheung, C. L., Woolley, A. T., and Lieber, C. M. (2001). Structural and functional imaging with carbon nanotube AFM probes. *Prog Biophys Mol Biol* 77:73–110.

Halford, S. E., Welsh, A. J., and Szczelkun, M. D. (2004). Enzyme-mediated DNA looping. *Annu Rev Biophys Biomol Struct* 33:1–24.

Hall, M. C., Shcherbakova, P. V., Fortune, J. M., Borchers, C. H., Dial, J. M., Tomer, K. B., and Kunkel, T. A. (2003). DNA binding by yeast Mlh1 and Pms1: implications for DNA mismatch repair. *Nucleic Acids Res* 31:2025–2034.

Hall, M. C., Wang, H., Erie, D. A., and Kunkel, T. A. (2001). High affinity cooperative DNA binding by the yeast Mlh1–Pms1 heterodimer. *J Mol Biol* 312:637–647.

Han, W., Lindsay, S. M., and Jing, T. (1996). A magnetically driven oscillating probe microscope for operation in fluids. *Appl Phys Lett* 69:4111–4114.

Hansma, H. G. (2001). Surface biology of DNA by atomic force microscopy. *Annu Rev Phys Chem* 52:71–92.

Hansma, H. G., Kasuya, K., and Oroudjev, E. (2004). Atomic force microscopy imaging and pulling of nucleic acids. *Curr Opin Struct Biol* 14:380–385.

Hansma, H. G. and Laney, D. E. (1996). DNA binding to mica correlates with cationic radius: assay by atomic force microscopy. *Biophys J* 70:1933–1939.

Hansma, P. K., Elings, V. B., Marti, O., and Bracker, C. E. (1988). Scanning tunneling microscopy and atomic force microscopy: application to biology and technology. *Science* 242:209–216.

Heddle, J. G., Mitelheiser, S., Maxwell, A., and Thomson, N. H. (2004). Nucleotide binding to DNA gyrase causes loss of DNA wrap. *J Mol Biol* 337:597–610.

Heinz, W. F. and Hoh, J. H. (1999). Spatially resolved force spectroscopy of biological surfaces using the atomic force microscope. *Trends Biotechnol* 17:143–150.

Henderson, R. M., Edwardson, J. M., Geisse, N. A., and Saslowsky, D. E. (2004). Lipid rafts: feeling is believing. *News Physiol Sci* 19:39–43.

Henn, A., Medalia, O., Shi, S. P., Steinberg, M., Franceschi, F., and Sagi, I. (2001). Visualization of unwinding activity of duplex RNA by DbpA, a DEAD box helicase, at single-molecule resolution by atomic force microscopy. *Proc Natl Acad Sci USA* 98:5007–5012.

Hoyt, P. R., Doktycz, M. J., Warmack, R. J., and Allison, D. P. (2001). Spin-column isolation of DNA-protein interactions from complex protein mixtures for AFM imaging. *Ultramicroscopy* 86:139–143.

Ikai, A. and Afrin, R. (2003). Toward mechanical manipulations of cell membranes and membrane proteins using an atomic force microscope: an invited review. *Cell Biochem Biophys* 39:257–277.

Janicijevic, A., Ristic, D., and Wyman, C. (2003a). The molecular machines of DNA repair: scanning force microscopy analysis of their architecture. *J Microsc* 212:264–272.

Janicijevic, A., Sugasawa, K., Shimizu, Y., Hanaoka, F., Wijgers, N., Djurica, M., Hoeijmakers, J. H., and Wyman, C. (2003b). DNA bending by the human damage recognition complex XPC-HR23B. *DNA Repair (Amst)* 2:325–336.

Jena, B. P. (2004). Discovery of the Porosome: revealing the molecular mechanism of secretion and membrane fusion in cells. *J Cell Mol Med* 8:1–21.

Jiao, Y., Cherny, D. I., Heim, G., Jovin, T. M., and Schaffer, T. E. (2001). Dynamic interactions of p53 with DNA in solution by time-lapse atomic force microscopy. *J Mol Biol* 314:233–243.

Kassies, R., van der Werf, K. O., Lenferink, A., Hunter, C. N., Olsen, J. D., Subramaniam, V., and Otto, C. (2005). Combined AFM and confocal fluorescence microscope for applications in bionanotechnology. *J Microsc* 217:109–116.

Kepert, J. F., Toth, K. F., Caudron, M., Mucke, N., Langowski, J., and Rippe, K. (2003). Conformation of reconstituted mononucleosomes and effect of linker histone H1 binding studied by scanning force microscopy. *Biophys J* 85:4012–4022.

Kolodner, R. D. and Marsischky, G. T. (1999). Eukaryotic DNA mismatch repair. *Curr Opin Genet Dev* 9:89–96.

Leckband, D. (2000). Measuring the forces that control protein interactions. *Annu Rev Biophys Biomol Struct* 29:1–26.

Lee, C. S. and Belfort, G. (1989). Changing activity of ribonuclease A during adsorption: a molecular explanation. *Proc Natl Acad Sci USA* 86:8392–8396.

Leuba, S. H., Bennink, M. L., and Zlatanova, J. (2004). Single-molecule analysis of chromatin. *Methods Enzymol* 376:73–105.

Li, J., Zhu, M., Manning-Bog, A. B., Di Monte, D. A., and Fink, A. L. (2004). Dopamine and L-dopa disaggregate amyloid fibrils: implications for Parkinson's and Alzheimer's disease. *Faseb J* 18: 962–964.

Liphardt, J., Onoa, B., Smith, S. B., Tinoco, I. J., and Bustamante, C. (2001). Reversible unfolding of single RNA molecules by mechanical force. *Science* 292:733–737.

Luckham, P. F. and Smith, K. (1998). Direct measurement of recognition forces between proteins and membrane receptors. *Faraday Discuss* 307–320; discussion 331–343.

Lushnikov, A. Y., Brown, B. A. II, Oussatcheva, E. A., Potaman, V. N., Sinden, R. R., and Lyubchenko, Y. L. (2004). Interaction of the Zalpha domain of human ADAR1 with a negatively supercoiled plasmid visualized by atomic force microscopy. *Nucleic Acids Res* 32:4704–4712.

Lynch, M., Mosher, C., Huff, J., Nettikadan, S., Johnson, J., and Henderson, E. (2004). Functional protein nanoarrays for biomarker profiling. *Proteomics* 4:1695–1702.

Lysetska, M., Knoll, A., Boehringer, D., Hey, T., Krauss, G., and Krausch, G. (2002). UV light-damaged DNA and its interaction with human replication protein A: an atomic force microscopy study. *Nucleic Acids Res* 30:2686–2691.

Lyubchenko, Y. L., Gall, A. A., Shlyakhtenko, L. S., Harrington, R. E., Jacobs, B. L., Oden, P. I., and Lindsay, S. M. (1992). Atomic force microscopy imaging of double stranded DNA and RNA. *J Biomol Struct Dyn* 10:589–606.

Lyubchenko, Y. L., Jacobs, B. L., Lindsay, S. M., and Stasiak, A. (1995). Atomic force microscopy of nucleoprotein complexes. *Scanning Microsc* 9:705–724; discussion 724–727.

Lyubchenko, Y. L., Oden, P. I., Lampner, D., Lindsay, S. M., and Dunker, K. A. (1993). Atomic force microscopy of DNA and bacteriophage in air, water and propanol: the role of adhesion forces. *Nucleic Acids Res* 21:1117–1123.

Marti, O., Elings, V., Haugan, M., Bracker, C. E., Schneir, J., Drake, B., Gould, S. A., Gurley, J., Hellemans, L., Shaw, K., *et al*. (1988). Scanning probe microscopy of biological samples and other surfaces. *J Microsc* 152 (Pt 3):803–809.

McGrew, D. A., and Knight, K. L. (2003). Molecular design and functional organization of the RecA protein. *Crit Rev Biochem Mol Biol* 38:385–432.

Modrich, P. and Lahue, R. (1996). Mismatch repair in replication fidelity, genetic recombination, and cancer biology. *Annu Rev Biochem* 65:101–133.

Moreno-Herrero, F., Colchero, J., Gomez-Herrero, J., and Baro, A. M. (2004). Atomic force microscopy contact, tapping, and jumping modes for imaging biological samples in liquids. *Phys Rev E Stat Nonlin Soft Matter Phys* 69:031915.

Mou, J., Czajkowsky, D. M., Zhang, Y., and Shao, Z. (1995). High-resolution atomic-force microscopy of DNA: the pitch of the double helix. *FEBS Lett* 371:279–282.

Muller, D. J., Amrein, M., and Engel, A. (1997). Adsorption of biological molecules to a solid support for scanning probe microscopy. *J Struct Biol* 119:172–188.

Muller, D. J., Dencher, N. A., Meier, T., Dimroth, P., Suda, K., Stahlberg, H., Engel, A., Seelert, H., and Matthey, U. (2001). ATP synthase: constrained stoichiometry of the transmembrane rotor. *FEBS Lett* 504:219–222.

Muller, D. J. and Engel, A. (1997). The height of biomolecules measured with the atomic force microscope depends on electrostatic interactions. *Biophys J* 73:1633–1644.

Muller, D. J., Fotiadis, D., and Engel, A. (1998). Mapping flexible protein domains at subnanometer resolution with the atomic force microscope. *FEBS Lett* 430:105–111.

Muller, D. J., Fotiadis, D., Scheuring, S., Muller, S. A., and Engel, A. (1999). Electrostatically balanced subnanometer imaging of biological specimens by atomic force microscope. *Biophys J* 76:1101–1111.

Mysiak, M. E., Bleijenberg, M. H., Wyman, C., Holthuizen, P. E., and van der Vliet, P. C. (2004a). Bending of adenovirus origin DNA by nuclear factor I as shown by scanning force microscopy is required for optimal DNA replication. *J Virol* 78:1928–1935.

Mysiak, M. E., Wyman, C., Holthuizen, P. E., and van der Vliet, P. C. (2004b). NFI and Oct-1 bend the Ad5 origin in the same direction leading to optimal DNA replication. *Nucleic Acids Res* 32:6218–6225.

Oberleithner, H., Schillers, H., Wilhelmi, M., Butzke, D., and Danker, T. (2000). Nuclear pores collapse in response to CO2 imaged with atomic force microscopy. *Pflugers Arch* 439:251–255.

Oberleithner, H., Schneider, S., and Bustamante, J. O. (1996). Atomic force microscopy visualizes ATP-dependent dissociation of multimeric TATA-binding protein before translocation into the cell nucleus. *Pflugers Arch* 432:839–844.

Ohnesorge, F. M., Horber, J. K., Haberle, W., Czerny, C. P., Smith, D. P., and Binnig, G. (1997). AFM review study on pox viruses and living cells. *Biophys J* 73:2183–2194.

Osmulski, P. A. and Gaczynska, M. (2000). Atomic force microscopy reveals two conformations of the 20 S proteasome from fission yeast. *J Biol Chem* 275:13171–13174.

Podesta, A., Imperadori, L., Colnaghi, W., Finzi, L., Milani, P., and Dunlap, D. (2004). Atomic force microscopy study of DNA deposited on poly L-ornithine-coated mica. *J Microsc* 215:236–240.

Radmacher, M., Tillamnn, R. W., Fritz, M., and Gaub, H. E. (1992). From molecules to cells: imaging soft samples with the atomic force microscope. *Science* 257:1900–1905.

Rakowska, A., Danker, T., Schneider, S. W., and Oberleithner, H. (1998). ATP-Induced shape change of nuclear pores visualized with the atomic force microscope. *J Membr Biol* 163:129–136.

Ratcliff, G. C. and Erie, D. A. (2001). A novel single-molecule study to determine protein–protein association constants. *J Am Chem Soc* 123:5632–5635.

Ratcliff, G. C., Erie, D. A., and Superfine, R. (1998). Photothermal modulation for oscillating mode atomic force microscopy in solution. *Appl Phys Lett* 72:1911–1913.

Rees, W. A., Keller, R. W., Vesenka, J. P., Yang, G., and Bustamante, C. (1993). Evidence of DNA bending in transcription complexes imaged by scanning force microscopy. *Science* 260: 1646–1649.

Rippe, K., Guthold, M., von Hippel, P. H., and Bustamante, C. (1997). Transcriptional activation via DNA-looping: visualization of intermediates in the activation pathway of *E. coli* RNA polymerase x sigma 54 holoenzyme by scanning force microscopy. *J Mol Biol* 270:125–138.

Rivetti, C., Codeluppi, S., Dieci, G., and Bustamante, C. (2003). Visualizing RNA extrusion and DNA wrapping in transcription elongation complexes of bacterial and eukaryotic RNA polymerases. *J Mol Biol* 326:1413–1426.

Rivetti, C., Guthold, M., and Bustamante, C. (1996). Scanning force microscopy of DNA deposited onto mica: equilibration versus kinetic trapping studied by statistical polymer chain analysis. *J Mol Biol* 264:919–932.

Rivetti, C., Guthold, M., and Bustamante, C. (1999). Wrapping of DNA around the *E. coli* RNA polymerase open promoter complex. *EMBO J* 18:4464–4475.

Rogers, B., Manning, L., Sulchek, T., and Adams, J. D. (2004). Improving tapping mode atomic force microscopy with piezoelectric cantilevers. *Ultramicroscopy* 100:267–276.

Ros, R., Eckel, R., Bartels, F., Sischka, A., Baumgarth, B., Wilking, S. D., Puhler, A., Sewald, N., Becker, A., and Anselmetti, D. (2004). Single molecule force spectroscopy on ligand-DNA complexes: from molecular binding mechanisms to biosensor applications. *J Biotechnol* 112:5–12.

Rounsevell, R., Forman, J. R., and Clarke, J. (2004). Atomic force microscopy: mechanical unfolding of proteins. *Methods* 34:100–111.

Safinya, C. R. (2001). Structures of lipid-DNA complexes: supramolecular assembly and gene delivery. *Curr Opin Struct Biol* 11:440–448.

Sato, M. H., Ura, K., Hohmura, K. I., Tokumasu, F., Yoshimura, S. H., Hanaoka, F., and Takeyasu, K. (1999). Atomic force microscopy sees nucleosome positioning and histone H1-induced compaction in reconstituted chromatin. *FEBS Lett* 452:267–271.

Sattin, B. D. and Goh, M. C. (2004). Direct observation of the assembly of RecA/DNA complexes by atomic force microscopy. *Biophys J* 87:3430–3436.

Schlacher, K., Leslie, K., Wyman, C., Woodgate, R., Cox, M. M., and Goodman, M. F. (2005). DNA polymerase V and RecA protein, a minimal mutasome. *Mol Cell* 17:561–572.

Schneider, S. W., Larmer, J., Henderson, R. M., and Oberleithner, H. (1998). Molecular weights of individual proteins correlate with molecular volumes measured by atomic force microscopy. *Pflugers Arch* 435:362–367.

Seitz, E. M., Brockman, J. P., Sandler, S. J., Clark, A. J., and Kowalczykowski, S. C. (1998). RadA protein is an archaeal RecA protein homolog that catalyzes DNA strand exchange. *Genes Dev* 12:1248–1253.

Shao, Z., Shi, D., and Somlyo, A. V. (2000). Cryoatomic force microscopy of filamentous actin. *Biophys J* 78:950–958.

Shao, Z. and Zhang, Y. (1996). Biological cryo atomic force microscopy: a brief review. *Ultramicroscopy* 66:141–152.

Sheng, S., Gao, Y., Khromov, A. S., Somlyo, A. V., Somlyo, A. P., and Shao, Z. (2003). Cryo-atomic force microscopy of unphosphorylated and thiophosphorylated single smooth muscle myosin molecules. *J Biol Chem* 278:39892–39896.

Sheng, S. and Shao, Z. (2002). Cryo-atomic force microscopy. *Methods Cell Biol* 68:243–256.

Shlyakhtenko, L. S., Gall, A. A., Filonov, A., Cerovac, Z., Lushnikov, A., and Lyubchenko, Y. L. (2003). Silatrane-based surface chemistry for immobilization of DNA, protein-DNA complexes and other biological materials. *Ultramicroscopy* 97:279–287.

Sincell, M. (2000). NanoManipulator lets chemists go Mano to Nano with molecules. *Science* 290: 1530.

Smith, G. C., Cary, R. B., Lakin, N. D., Hann, B. C., Teo, S. H., Chen, D. J., and Jackson, S. P. (1999). Purification and DNA binding properties of the ataxia-telangiectasia gene product ATM. *Proc Natl Acad Sci USA* 96:11134–11139.

Stahlberg, H., Fotiadis, D., Scheuring, S., Remigy, H., Braun, T., Mitsuoka, K., Fujiyoshi, Y., and Engel, A. (2001). Two-dimensional crystals: a powerful approach to assess structure, function and dynamics of membrane proteins. *FEBS Lett* 504:166–172.

Stevens, R. M. D., Frederick, N. A., Smith, B. L., Morse, D. E., Stucky, G. D., and Hansma, P. K. (2000). Carbon nanotubes as probes for atomic force microscopy. *Nanotechnology* 11:1–5.

Stoffler, D., Goldie, K. N., Feja, B., and Aebi, U. (1999). Calcium-mediated structural changes of native nuclear pore complexes monitored by time-lapse atomic force microscopy. *J Mol Biol* 287:741–752.

Stolz, M., Stoffler, D., Aebi, U., and Goldsbury, C. (2000). Monitoring biomolecular interactions by time-lapse atomic force microscopy. *J Struct Biol* 131:171–180.

Tamayo, J. (2003a). Structure of human chromosomes studied by atomic force microscopy. *J Struct Biol* 141:198–207.

Tamayo, J. (2003b). Structure of human chromosomes studied by atomic force microscopy. Part II. Relationship between structure and cytogenetic bands. *J Struct Biol* 141:189–197.

Tessmer, I., Moore, T., Lloyd, R. G., Wilson, A., Erie, D. A., Allen, S., and Tendler, S. J. (2005). AFM studies on the role of the protein RdgC in bacterial DNA recombination. *J Mol Biol* 350:254–262.

Tokunaga, M., Aoki, T., Hiroshima, M., Kitamura, K., and Yanagida, T. (1997). Subpiconewton intermolecular force microscopy. *Biochem Biophys Res Commun* 231:566–569.

Umemura, K., Komatsu, J., Uchihashi, T., Choi, N., Ikawa, S., Nishinaka, T., Shibata, T., Nakayama, Y., Katsura, S., Mizuno, A., Tokumoto, H., Ishikawa, M., and Kuroda, R. (2001). Atomic force microscopy of RecA–DNA complexes using a carbon nanotube tip. *Biochem Biophys Res Commun* 281:390–395.

van Noort, J., Orsini, F., Eker, A., Wyman, C., de Grooth, B., and Greve, J. (1999). DNA bending by photolyase in specific and non-specific complexes studied by atomic force microscopy. *Nucleic Acids Res* 27:3875–3880.

Verhoeven, E. E., Wyman, C., Moolenaar, G. F., and Goosen, N. (2002). The presence of two UvrB subunits in the UvrAB complex ensures damage detection in both DNA strands. *EMBO J* 21:4196–4205.

Verhoeven, E. E., Wyman, C., Moolenaar, G. F., Hoeijmakers, J. H., and Goosen, N. (2001). Architecture of nucleotide excision repair complexes: DNA is wrapped by UvrB before and after damage recognition. *EMBO J* 20:601–611.

Viani, M. B., Schaffer, T. E., Chand, A., Rief, M., Gaub, H. E., and Hansma, P. K. (1999). Small cantilevers for force spectroscopy of single molecules. *J Appl Phys* 86:2258–2262.

Vickery, S. A. and Dunn, R. C. (2001). Combining AFM and FRET for high resolution fluorescence microscopy. *J Microsc* 202:408–412.

Wagner, P. (1998). Immobilization strategies for biological scanning probe microscopy. *FEBS Lett* 430:112–115.

Wang, H. (2003). Atomic force microscopy studies of initiation events in DNA mismatch repair: In *Matls Sci*, University of North Carolina at Chapel Hill, Chapel Hill.

Wang, H., Yang, Y., Schofield, M. J., Du, C., Fridman, Y., Lee, S. D., Larson, E. D., Drummond, J. T., Alani, E., Hsieh, P., and Erie, D. A. (2003). DNA bending and unbending by MutS govern mismatch recognition and specificity. *Proc Natl Acad Sci USA* 100:14822–14827.

Willemsen, O. H., Snel, M. M., Cambi, A., Greve, J., De Grooth, B. G., and Figdor, C. G. (2000). Biomolecular interactions measured by atomic force microscopy. *Biophys J* 79:3267–3281.

Wolberg, A. S., Stafford, D. W., and Erie, D. A. (1997). Human factor IX binds to specific sites on the collagenous domain of collagen IV. *J Biol Chem* 272:16717–16720.

Woolley, A. T., Cheung, C. L., Hafner, J. H., and Lieber, C. M. (2000). Structural biology with carbon nanotube AFM probes. *Chem Biol* 7:193–204.

Wyman, C., Rombel, I., North, A. K., Bustamante, C., and Kustu, S. (1997). Unusual oligomerization required for activity of NtrC, a bacterial enhancer-binding protein. *Science* 275:1658–1661.

Xu, H. and Hoover, T. R. (2001). Transcriptional regulation at a distance in bacteria. *Curr Opin Microbiol* 4:138–144.

Xue, Y., Ratcliff, G. C., Wang, H., Davis-Searles, P. R., Gray, M. D., Erie, D. A., and Redinbo, M. R. (2002). A minimal exonuclease domain of WRN forms a hexamer on DNA and possesses both 3′– 5′ exonuclease and 5′-protruding strand endonuclease activities. *Biochemistry* 41:2901–2912.

Yaneva, M., Kowalewski, T., and Lieber, M. R. (1997). Interaction of DNA-dependent protein kinase with DNA and with Ku: biochemical and atomic-force microscopy studies. *EMBO J* 16:5098–5112.

Yang, Y., Sass, L. E., Du, C., Hsieh, P., and Erie, D. A. (2005). Determination of protein-DNA binding constants and specificities from statistical analyses of single molecules: MutS-DNA interactions. *Nucleic Acids Res* 33:4322–4334.

Yang, Y., Wang, H., and Erie, D. A. (2003). Quantitative characterization of biomolecular assemblies and interactions using atomic force microscopy. *Methods* 29:175–187.

Yin, H., Wang, M. D., Svoboda, K., Landick, R., Block, S. M., and Gelles, J. (1995). Transcription against an applied force. *Science* 270:1653–1657.

Yoshimura, S. H., Maruyama, H., Ishikawa, F., Ohki, R., and Takeyasu, K. (2004). Molecular mechanisms of DNA end-loop formation by TRF2. *Genes Cells* 9:205–218.

Zelphati, O., Liang, X., Nguyen, C., Barlow, S., Sheng, S., Shao, Z., and Felgner, P. L. (2000). PNA-dependent gene chemistry: stable coupling of peptides and oligonucleotides to plasmid DNA. *Biotechniques* 28:304–310, 312–314, 316.

Zhang, Q., Powers, E. T., Nieva, J., Huff, M. E., Dendle, M. A., Bieschke, J., Glabe, C. G., Eschenmoser, A., Wentworth, P., Jr., Lerner, R. A., and Kelly, J. W. (2004). Metabolite-initiated protein misfolding may trigger Alzheimer's disease. *Proc Natl Acad Sci USA* 101:4752–4257.

Zhuang, X. and Rief, M. (2003). Single-molecule folding. *Curr Opin Struct Biol* 13:88–97.

Zlatanova, J. and Leuba, S. H. (2003). Chromatin fibers, one-at-a-time. *J Mol Biol* 331:1–19.

Zlatanova, J., Lindsay, S. M., and Leuba, S. H. (2000). Single molecule force spectroscopy in biology using the atomic force microscope. *Prog Biophys Mol Biol* 74:37–61.

http://www.springer.com/978-0-387-35965-6

Protein Interactions
Biophysical Approaches for the Study of Complex Reversible Systems
(Ed.)P. Schuck
2007, XI, 532 p., Hardcover
ISBN: 978-0-387-35965-6